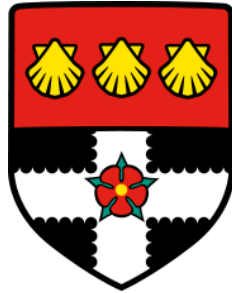


UNIVERSITY OF READING

Department of Mathematics



Computer Simulations of Dipolar Fluids
Using Ewald Summations

Naomi J. K. Withey

August 2012

This is a dissertation submitted in partial fulfilment of the requirement
for the degree of Master of Science.

Abstract

The Ewald summation method is a key way to improve the accuracy of computer simulations, which are essential in building our understanding of the behaviour of dipolar substances, particularly magnetic fluids. Implementation and accuracy in a three dimensional periodic geometry are discussed comprehensively, drawing together many of the key publications in this field. The procedure is then extended to account for the confined geometry representative of thin layers of ferrofluids. This is done using the EW3DLC method, which allows us to work with a three dimensional system that is periodic in only two directions.

Acknowledgements

I would firstly like to thank Reading University Department of Mathematics for the scholarship that has funded my studies over the past year. As I didn't need to find the extra money for fees I was able to live in more comfort than I would have otherwise been able to! I would also like to thank the staff in the department for their continued support throughout the year. Particular thanks go to Dr. Peter Sweby and Professor Mike Baines for answering my many questions as well as others who are too numerous to mention.

In relation to this project I would like to thank Dr. Zuowei Wang for sparking my interest in this topic and for his support as supervisor. I am also grateful to him for letting me use programs he had written as part of his previous explorations of this subject, especially having seen how many elements there are to the programs involved!

Last but definitely not least I would like to thank the family and friends that have given me their support. Special thanks go to my mum, dad and siblings; John, Jake and Mog; for their love and support throughout my academic career to date. I couldn't have got this far without them. Thanks also goes to Sarah, James, Tom, Ash, Jack, Jon, Chris, Jason and the many others who provided cups of tea, kept me smiling and made sure I kept a foot in the world outside the maths building. Special thanks goes to Alex for having faith in my abilities when I didn't and putting up with me constantly moaning about how much work I had to do.

Declaration

I confirm that this is my own work, and the use of all material from other sources has been properly and fully acknowledged.

Signed

Contents

1	Introduction	1
1.1	Dipolar Interactions	1
1.2	Applications of Magnetic Fluids	2
1.3	Project Aims	3
2	Molecular Dynamics	4
2.1	Finite Differences Methods	5
2.1.1	The Leapfrog Method	5
2.2	Long Range Interactions	7
3	Ewald Summations	9
3.1	Derivation of Ewald Summations	9
3.1.1	Charge-Charge Interactions	10
3.1.2	Dipole-Dipole Interactions	15
3.1.3	Fast Fourier Transforms	17
3.2	Application of Ewald Summations	19
3.2.1	Force	20
3.2.2	Torque	22
3.3	Errors in Ewald Summations	24
3.3.1	Errors in Real Space	25
3.3.2	Errors in Reciprocal Space	28
3.3.3	Optimising the Parameters	30
4	Simulation	32
4.1	Average Cluster Size	32
5	Dealing with a Confined Geometry	36
5.1	What is a Confined Geometry?	36
5.2	Ewald Method for a Confined Geometry	37
5.2.1	Charge-Charge Interactions	37
5.2.2	Dipole-Dipole Interactions	39
5.3	Application of Ewald Method for a Confined Geometry	41
5.3.1	Force	41
5.3.2	Torque	43
5.4	Errors in Ewald Method for a Confined Geometry	45
6	Conclusion	48
6.1	Further Work	48

Appendix A List of Symbols **i**

 A.1 Latin Alphabet i

 A.2 Greek Alphabet ii

Appendix B Glossary **iv**

References **vi**

1 Introduction

Owing to the complex nature of molecular systems the ability to model them effectively using computers is increasingly important. Computer simulations allow macroscopic systems to be modelled on a microscopic level by studying the intermolecular interactions contained within. Thus computers allow us to find solutions where analytical methods fail and compare them to results obtained experimentally. In this way simulation aims to bridge the gap between experimental and theoretical physics. Clearly the size of the system being modelled is restricted by the available storage on the host computer and the speed with which the program can be run.

The method of molecular dynamics coupled with the application of periodic boundary conditions (PBCs) allows larger systems to be modelled at reduced computing costs. An efficient use is made of these in the implementation of the Ewald summation when dealing with long range interactions, which can easily be adapted to allow its application to a variety of scenarios.

The Ewald method was established in 1921 by Paul Peter Ewald, a US crystallographer (although German by birth), who used it to determine the electrostatic energies of ionic crystals. It has since been developed for other uses and is the most commonly used technique when dealing with many-body systems that have periodic boundary conditions. A particular advantage it has over other methods is its ability to employ fast Fourier transforms (FFTs) to drastically reduce computing requirements in simulations.

1.1 Dipolar Interactions

Many of the most interesting molecular systems are charged systems such as those governed by dipole-dipole interactions. These electrostatic interactions can have important biological consequences since water, which is a dipolar substance, is contained in all biological tissues^[33]. They are also essential in the modelling of ferrofluids and magnetorheological (MR) fluids, which are colloidal liquids consisting of small magnetic particles dispersed in a solvent. Such fluids become strongly magnetised when under the influence of an external magnetic field, although the changes undergone are reversible and the substances return to their original states once the field is no longer present. Simulations of such fluids illustrate the tendency of the particles to form chains aligned with the magnetic field as demonstrated in Figure 1. Furthermore, these chains combine to create labyrinthine structures (see Figure 2) where the complexity of the pattern is dependent on the density of the particles and the restraints of the system in the direction of the external field^[26]. With such interesting properties it is no wonder that magnetic fluids have attracted the interest of scientists from many different fields.

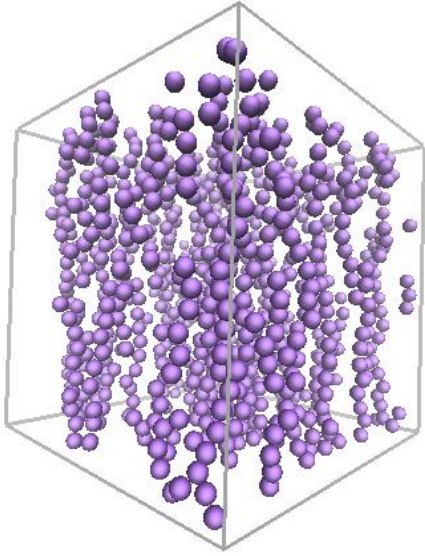


Figure 1: Side view of particles to illustrate chain formation in the direction of the magnetic field.

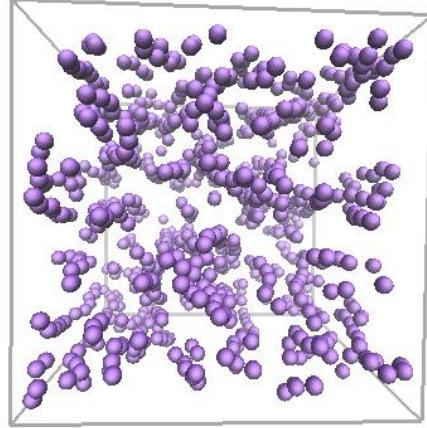


Figure 2: View of particles from above to demonstrate labyrinthine structure.

In the late 1990s and early 2000s researchers were fascinated by the structures exhibited and published works modelling this behaviour^[19,26,35]. It was then that the effectiveness of Ewald summations in this area was first investigated^[35]. Due to the long range nature of dipole-dipole interactions Ewald summations (as derived rigorously by De Leeuw et al.^[11]) provided more accurate results, as verified by the error calculations performed by Wang and Holm^[33], as well as reducing computational requirements. Since then work has begun to simulate the behaviours of magnetic fluids in a slab geometry where the system is confined in one direction^[5,7,15]. This extension into a confined geometry is of key interest in current studies.

In 2007 Ivanov et al.^[20] wrote a comprehensive critique comparing experiment, theory and computer simulation in the modelling of ferrofluids, comparing the methodologies of much of the published work in this field. They praise molecular dynamics simulations for their reliability and considerations of computational convenience and efficiency. However, they do recognise its sensitivity to the method of discretisation and numerical integration used.

1.2 Applications of Magnetic Fluids

A key difference between ferrofluids and magneto-rheological fluids is the size of the magnetic particles, which are smaller (nanoscale) in ferrofluids than in MR fluids (microscale). Furthermore, permanent magnetic dipole moments are inherent in ferrofluids, whereas in MR fluids the magnetic properties are induced by an external field. Hence, ferrofluid

particles remain suspended in Brownian motion under normal conditions whereas those in MR fluids settle over time as they are denser than their surrounding fluid. As a result the two types of magnetic fluid have very different applications.

The colloidal properties of ferrofluids (the possession of properties of both the liquid and solid states of matter) allow them to be used as seals and lubricants. In particular, they form liquid seals around the spinning drive shafts in hard disks. They also have numerous medical applications including cancer detection and treatment, hypothermia treatment, targeted drug delivery and retina repairs^[10,22,24]. Rich et al.^[31] recently expressed hope that ferrofluids may continue to be exploited in the creation of materials with unique electrical or optical properties (for example, optical tweezers). MR fluids, on the other hand, are used in the automotive and aerospace industries in devices such as dampers, shock absorbers, clutches and brakes^[16]. They also have military applications in the development of enhanced body armour.

Due to the sensitive nature, and hence the accuracy required, of many of these applications a thorough understanding of the microstructure of magnetic fluids and how it affects the macroscopic properties is important. For this reason, the ability to model magnetic fluids continues to be an area of interest for many scientists from different disciplines. Simulations are particularly beneficial when new ferrofluids are discovered, such as those detailed by López-López et al.^[25], since the ability to model them can prelude control of their magnetic properties and lead to further applications being developed.

1.3 Project Aims

Initially this report reviews existing literature concerning computer simulations of dipolar interactions in order to gain an understanding of the application of molecular dynamics in this field (§2). In particular, we will study the mathematics behind Ewald summations and their role in optimising the performance of simulations (§3). In §4 the Ewald model discussed in §3 will be used to run simulations of fascinating dipolar systems, namely ferrofluids. This will be carried out by specifying initial positions for the particles and then tracking their movement over time as the simulation runs using existing programs. Finally, the methods discussed throughout this project will then be extended to represent a slab geometry rather than the standard three dimensional system (§5).

2 Molecular Dynamics

Molecular dynamics is a method for solving Newton's laws of motion that is used in computer simulations of molecular behaviours where intermolecular potentials are involved^[1,17]. It can be used to compute the properties of a classical¹ many-body system,^[12] such as temperature, energy and shear viscosity^[28]. The result is a path tracking the movement (positions and velocities) of the particles in a system over time. The method was developed in the late 1950s and in the first instances it was assumed that the particles moved with constant velocity allowing problems to be solved easily without making approximations (within computational limits). In the early 1960s this work was developed to model systems in which the forces involved change as the particles move^[1,17,23]. The first simulation of a fluid was performed in 1971.

Newton's second law of motion is stated in the box below:

The net force, \mathbf{F} , acting on a particle is directly proportional to and in the same direction as the acceleration, \mathbf{a} , of the particle and the acceleration is inversely proportional to the mass, m , of the particle ($\mathbf{a} = \frac{\mathbf{F}}{m}$).

It is the differential equations implicit in this law that are utilised in molecular dynamics^[23]:

$$\frac{d^2x}{dt^2} = \frac{F_x}{m}. \quad (1)$$

The equation (1) is solved for our sample of N particles until the properties of the system reach equilibrium^[12]. In this way we can study the behaviour of the particles in the system over time.

Molecular dynamics can be used in a variety of ways depending on the property of interest and the system being modelled. The method to be applied for this project can be broken down into the following steps^[12,14]:

1. Set up a random configuration of initial positions and velocities for the set of particles being modelled (initial conditions).
2. Calculate the force acting on each particle using the formula derived in §3.2.1.
3. Use numerical methods to integrate Newton's law and hence compute the positions and velocities of particles at the next time step.
4. Repeat steps 2 and 3 until the required situation is achieved.

Step 2 is the most time consuming, and hence computationally expensive, part of the simulation since we need to consider the interaction between each particle and all of its

¹The use of 'classical' here means that the particles in the system adhere to the laws of classical mechanics^[12]

neighbours. Hence for a system of N particles there are $\frac{N(N-1)}{2}$ pairs to be evaluated and so the computation time is $\mathcal{O}(N^2)$, although there are techniques that can reduce this time to $\mathcal{O}(N)$ (when there are no long range interactions), $\mathcal{O}(N^{\frac{3}{2}})$ or at best $\mathcal{O}(N \log N)$ [12,28,33]. Step 3 involves finding the solution of a system of second order ordinary differential equations (ODEs) and is commonly done using finite difference methods, as discussed in §2.1.

2.1 Finite Differences Methods

In the system we are modelling we assume that the force on a particle changes as the position of the particle does, which results in the presence of pairwise potentials; these are discussed in more detail in §3.1. The basic idea behind finite difference methods is that the solution is broken down into time steps and at each time step the net force on each particle is calculated using the pairwise interactions of the particles. From the force we can calculate the positions and velocities of the particles at the next time step and hence use this to compute the force at the next step and so forth [1,23]. In this way the relevant equations are solved time step by time step.

There are many different finite difference methods and so it can be difficult to know which is the most appropriate to use. A major factor in this is the computational time and effort required as these can massively impact the cost of running the simulation. Leach [23] describes how algorithms that are normally expensive may allow a significantly larger time step to be used and thus actually be more cost effective in the end. This idea is echoed by Frenkel and Smit [12] who go on to say that accuracy is the most important consideration when choosing which method to use. Once a method has been selected it remains to choose an appropriate time step. Key considerations here are making sure that the time step is chosen to maintain stability of the system without compromising the accuracy of the result. In more complicated systems the time step can be varied across the total running time of the simulation.

2.1.1 The Leapfrog Method

In many mathematical applications finite difference methods are applied across a computational grid, with $x_j = j\Delta x$ being the discretisation with respect to space and $t^n = n\Delta t$ being the discretisation with respect to time. It is then assumed that the numerical solution at these grid points approximates the true solution at these positions, i.e. $u_j^n \approx u(j\Delta x, n\Delta t)$.

The leapfrog scheme is then derived by using the Mean Value Theorem to discretise the first derivatives with respect to space and time. The result when applied to the simple differential equation $u_t = -au_x$ (the linear advection equation) is as follows:

$$u_t|_j^n = \frac{u_j^{n+1} - u_j^{n-1}}{2\Delta t}, \quad u_x|_j^n = \frac{u_{j+1}^n - u_{j-1}^n}{2\Delta x}.$$

This gives the leapfrog scheme^[27,29]

$$\begin{aligned} u_j^{n+1} &= u_j^{n-1} - a \frac{\Delta t}{\Delta x} (u_{j+1}^n - u_{j-1}^n) \\ &= u_j^{n-1} - \nu (u_{j+1}^n - u_{j-1}^n) \end{aligned}$$

where $\nu = a \frac{\Delta t}{\Delta x}$ is standard notation. This can easily be transformed into the staggered leapfrog method by using information at half steps in space and time instead. The interesting name of the scheme comes from the fact that it makes use of the two time intervals surrounding u_j^n to calculate a central time difference but does not actually require any information to be given at this intermediate time step. This scheme is second order accurate in both space and time and is stable when $|\nu| \leq 1$ (Morton and Mayers^[27] and Press et al.^[29] give more rigorous analyses of the stability condition).

As this leapfrog scheme operates on three levels of the grid it requires a one level scheme to be used to start the process and gain enough information to get the leapfrog method started. For this reason other methods that have the same accuracy but only require information at two grid levels are sometimes preferred. However, such methods are significantly more complicated to apply.

In molecular dynamics simulations, however, there is only a discretisation over time (and not space) and so the leapfrog method, whilst essentially the same as the staggered method described above, is presented differently. It is an adaptation of the Verlet algorithm, which uses Taylor series approximations to the variables. In this case the key components are^[1,17,23]

$$\mathbf{r}^{n+1} = \mathbf{r}^n + \Delta t \mathbf{v}^{n+\frac{1}{2}} \quad (2)$$

$$\mathbf{v}^{n+\frac{1}{2}} = \mathbf{v}^{n-\frac{1}{2}} + \Delta t \mathbf{a}^n \quad (3)$$

where \mathbf{r} refers to position, \mathbf{v} represents velocity and \mathbf{a} is acceleration. In order to apply the leapfrog algorithm (3) is first used to calculate the velocity at time $t + \frac{1}{2}\Delta t$. This velocity is then used in (2) to calculate the position at the next time step. The velocity at the current time can be calculated by use of the central difference^[1,23]

$$\mathbf{v}^n = \frac{1}{2} \left[\mathbf{v}^{n+\frac{1}{2}} + \mathbf{v}^{n-\frac{1}{2}} \right].$$

Hinchliffe^[17] praises the accuracy and stability of the leapfrog method for use in molecular dynamics and recommends the time step $\Delta t = 10^{-15}$ s (a femtosecond). Allen and Tildesley^[1] credit the accuracy of the scheme to the fact that there is never the require-

ment to difference two large numbers to generate a small number, which would result in loss of precision.

In mathematics predictor-corrector methods tend to be favoured due to the accuracy gained. Such methods operate by using one scheme to perform a calculation and obtain a predicted value. This predicted value is then put into a second, more accurate, scheme to give a corrected value. However, in molecular dynamics simulations such a method is not computationally efficient as it increases the number of calculations that are required.

2.2 Long Range Interactions

Allen and Tildesley^[1] define long range forces to be those in which the spatial interaction decays at a rate no faster than r^{-d} , where r is the particular separation and d is the dimensionality of the system. Since dipole-dipole interactions in three dimensional space are approximated by r^{-3} they fall into this category. In §3.1 charge-charge interactions are discussed as an introduction to the Ewald method, which are approximated by r^{-1} and hence are long range too.

Such systems can be difficult to represent computationally since for a typical simulation the interaction range of the molecules is much larger than half of the simulation box length. The solution is not as simple as increasing the box size as this would make the cost and computing time required to run a simulation far too great. There are 2 key problems, as described by Hinchliffe^[17]; the molecules at the edge of the box will be under the influence of different forces to those in a more central position and also, over time, molecules may leave the simulation box and thus reduce the density within.

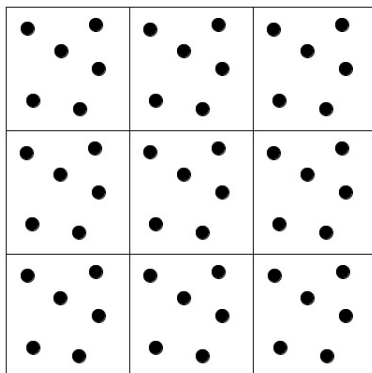


Figure 3: Simplified representation of two-dimensional slice of periodic boxes.

These issues can be tackled by creating a system of adjoining simulation boxes that are identical on an atomic level, as demonstrated in Figure 3. Mathematically, this involves simulating the behaviour in one cell and applying periodic boundary conditions (PBCs) to it. So, if a molecule leaves the simulated space it will be replaced by its image entering from another box, hence maintaining the density. Furthermore, if we take a central cell, the molecules contained within will be interacting with every other molecule in that cell

and in the surrounding cells. This resolves the problem of varying influences due to the position of walls as we assume the system is infinite^[1,17]. Computing ability is enhanced since we are able to study a microscopic portion of the system and use the PBCs to extrapolate the results throughout the macroscopic system.

The interactions of a molecule with all of its periodic images can be modelled efficiently using Ewald summations^[1], which are described in detail in §3.

3 Ewald Summations

Since we have assumed an infinite system a cut-off needs to be decided in order to perform calculations, which introduces truncation errors to the model. This is where the Ewald summation proves to be most effective as it is designed to split the problem into two parts, both of which decay rapidly, and so the system can be truncated with much less loss of accuracy. Allen and Tildesley^[1] and Leach^[23] criticise the Ewald method for placing too much emphasis on the periodicity of the system being modelled. In particular, any temporary fluctuations in the molecular interactions are likely to be repeated periodically rather than being damped out. Computation of the reciprocal part of the Ewald summation is also expensive. However, use of the Ewald sum with an optimal splitting parameter and fast Fourier transforms (FFT) can reduce the computation time from $\mathcal{O}(N^2)$ to approximately $\mathcal{O}(N \log N)$, where N is the number of particles in a simulation box^[23,28,33]. Hence, the increase in efficiency outweighs the faults in the method for basic implementations.

Throughout this section the trigonometric definition of an exponential with an imaginary component is used to switch between the two formats and so it is stated here for convenience.

$$e^{ix} = \cos(x) + i \sin(x) \tag{4}$$

3.1 Derivation of Ewald Summations

Since the Ewald method was originally developed for charge-charge interactions (such as those in proteins and DNA) we begin by looking at these (§3.1.1) and then extend the method to derive the appropriate formulae for dipolar interactions (§3.1.2).

The derivations in this section are based on a cubic simulation box with sides of length L . It would be possible, and indeed trivial, to instead use a cuboid simulation box with dimensions $L_x \times L_y \times L_z$, much like the one discussed in §5.2.

In order to calculate the force on an individual molecule (and hence understand how it moves over time) we need to look at the inter-molecular interactions, which are modelled using potentials. Although, as detailed by Ogbonna^[28], the potentials in a system containing N particles can be split into terms depending on single particles, pairs of particles, triplets and so forth we only study pairwise interactions since they have the most significant contribution. These pairwise interactions depend on the distance between the two molecules, given by $\mathbf{r}_{ij} = \mathbf{r}_i - \mathbf{r}_j$, where \mathbf{r}_i and \mathbf{r}_j are vectors describing the positions of molecules i and j respectively. So, the total potential energy is a function of \mathbf{r}_{ij} determined by the system being modelled summed over all integer values of i and j from 1 to N . Furthermore, for the potential energy to be finite we assume that the system as a whole is electrically neutral^[12].

Coulomb's law (see Appendix B) describes the electrostatic interactions between par-

ticles in the manner discussed in the previous paragraph and includes a proportionality constant of $(4\pi\epsilon_0)^{-1}$, where ϵ_0 is the permittivity (a measure of resistance) of free space^[17]. Throughout this report all factors of $4\pi\epsilon_0$ have been omitted to make the notation compact, as is the convention. This equates to using Gaussian rather than SI units of charge; in this case charge will have units of $\text{mN}^{\frac{1}{2}}$ ^[1].

It is worth noting that the derivation of the Ewald summation takes the periodicity of the system into account by the use of the Fourier sum, so no further calculations are required to this end.

3.1.1 Charge-Charge Interactions

The total paired potential energy of a three dimensional periodic system involving charge-charge interactions can be written as ²

$$U_c = \frac{1}{2} \sum_{\mathbf{n}}' \left(\sum_{i=1}^N \sum_{j=1}^N \frac{q_i q_j}{|\mathbf{r}_{ij} + \mathbf{n}|} \right) \quad (5)$$

where q_i and q_j are two charges and the subscript c denotes that this is the derivation for charge-charge interactions^[1,23]. Also, $\mathbf{n} = (n_x L, n_y L, n_z L)$ for n_x, n_y, n_z integers and L the length of the simulation box so that this vector represents a cube. The notation $\sum_{\mathbf{n}}'$ signifies that the term where $i = j$ has been omitted when $\mathbf{n} = \mathbf{0}$. In other words each particle interacts with all other particles and all images of itself but doesn't interact with itself.

Since the result in (5) is conditionally convergent when dealing with long range interactions the result of the sum depends on the order terms are added in. A seemingly natural choice would be to start with the boxes closest to the central box and branch out in a roughly spherical manner, as demonstrated in Figure 4.

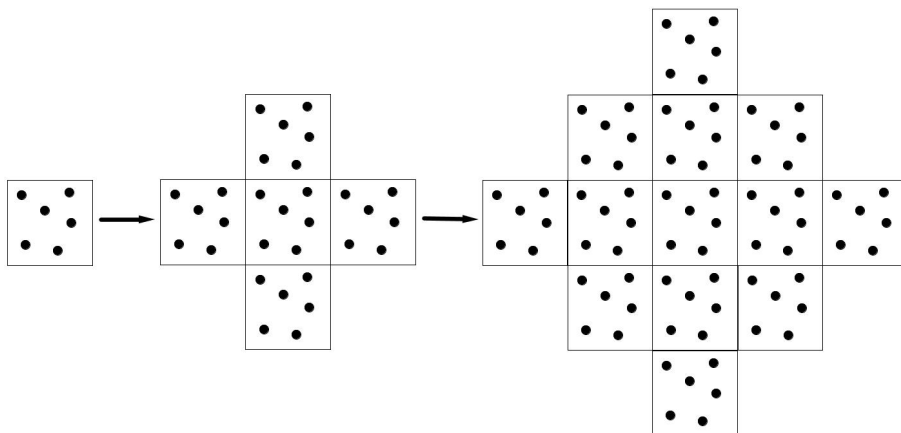


Figure 4: Simplified two-dimensional representation of the summation of periodic boxes.

²Remember that all factors of $4\pi\epsilon_0$ have been omitted.

The relative permittivity of the medium surrounding the sphere containing our summed boxes can differ vastly. For example, a system surrounded by a metal that conducts well has relative permittivity $\epsilon_s = \infty$ outside the sphere and outside a system surrounded by a vacuum we have $\epsilon_s = 1$. These two extremes are related in the following way

$$U_c(\epsilon_s = \infty) = U_c(\epsilon_s = 1) - \frac{2\pi}{3L^3} \left| \sum_i q_i \mathbf{r}_i \right|^2$$

when the size of the sphere of boxes is sufficiently large^[1]. Whilst the Ewald summation is an effective method of calculating $U_c(\epsilon_s = \infty)$ we are assuming that our system is surrounded by a vacuum, ($\epsilon_s = 1$), and therefore the surface term

$$U_c^{surf} = \frac{2\pi}{3L^3} \left| \sum_{i=1}^N q_i \mathbf{r}_i \right|^2 \quad (6)$$

needs to be added to our potential.

De Leeuw et al.^[11] (see also Smith and Perram^[32]) provide a detailed mathematical account of the derivation of the Ewald method. However, an in depth knowledge of various mathematical processes is required to fully understand this and so it is not recounted here. However, the principle idea behind the Ewald method is to convert the slow converging summation in (5) into two rapidly (and absolutely) converging components using the mathematical identity^[23]

$$\frac{1}{r} = \frac{f(r)}{r} + \frac{1-f(r)}{r}. \quad (7)$$

The first term on the right hand side of (7) will correspond to a summation in real space and the second term will be a summation in reciprocal space. This provides a more accurate result than just using the left hand side in its original state as the Fourier transform performed on the second term takes account of a much wider space.

Each charge is surrounded by a neutralising charge distribution as described in (8) that is assumed to be Gaussian.

$$\rho_{G1}^{charge}(r) = \frac{q_i \alpha^3 e^{-\alpha^2 r^2}}{\pi^{\frac{3}{2}}} \quad (8)$$

where α is an arbitrary splitting parameter describing the width of the distribution and $r = |\mathbf{r}| = |\mathbf{r}_{ij} + \mathbf{n}|$ gives the position in respect of the centre of the distribution^[1,12,23]. Taking this into account (5) becomes a sum of the pairwise interactions combined with these Gaussian distributions given by

$$U_c^r = \frac{1}{2} \sum_{\mathbf{n} \in \mathbb{Z}^3} \prime \left(\sum_{i=1}^N \sum_{j=1}^N q_i q_j \frac{erfc(\alpha |\mathbf{r}_{ij} + \mathbf{n}|)}{|\mathbf{r}_{ij} + \mathbf{n}|} \right) \quad (9)$$

where $\operatorname{erfc}(x) = \frac{2}{\sqrt{\pi}} \int_x^\infty e^{-t^2} dt$ is the complementary error function^[1,23], which tends to zero as x increases. Equation (9) gives the amended real space contribution to our potential.

We now have a system of screened charges, as illustrated in Figure 5, consisting of the point charges and the neutralising distribution. So, a second charge distribution needs to be introduced in order to counteract the Gaussian distribution added previously, as depicted in Figure 6 (i.e. Figures 5 and 6 combined leaves just the point charges we require)^[1,12,23,28].

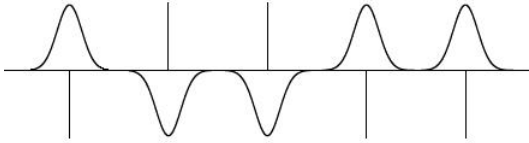


Figure 5: Screened charges.^[28]

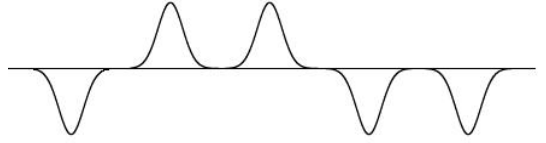


Figure 6: Cancelling distribution.^[28]

It may seem easier to simply ignore the contribution of the screening distribution. However, its inclusion means that the summation in (9) converges rapidly and so can be truncated with less loss of accuracy. The speed of convergence is dependent on the width of the Gaussian distribution in (8) as wider distributions will converge more quickly^[23]. This can be controlled by selecting an optimal value of the parameter α . A further important development is that we can now subtract a cancelling function which can be expressed as a rapidly converging Fourier series.³

In order to calculate the contribution from the cancelling charge distribution we start with the periodic sum of Gaussians in (10) at the position of \mathbf{r}_i ^[12].

$$\rho_{G2}^{charge}(r) = \sum_{j=1}^N \sum_{\mathbf{n}} \frac{q_j \alpha^3 e^{-\alpha^2 |\mathbf{r}_{ij} + \mathbf{n}|^2}}{\pi^{\frac{3}{2}}} \quad (10)$$

We then take the Fourier transform of (10) where $\mathbf{k} = \frac{2\pi\mathbf{n}}{L^2} = \frac{2\pi}{L^2}(k_x, k_y, k_z)$ for k_x, k_y, k_z integers is the corresponding vector in reciprocal space^[1,12,14,23].

³There is a slight abuse of notation in this derivation since i is taken to represent $\sqrt{-1}$ but subscript i still relates to the summation index, as in previous appearances.

$$\begin{aligned}
\hat{\rho}_{G2}^{charge}(\mathbf{k}) &= \frac{1}{L^3} \int_{L^3} \rho_{G2}^{charge}(\mathbf{r}) e^{-i\mathbf{k}\cdot\mathbf{r}} d\mathbf{r} \\
&= \frac{1}{L^3} \int_{L^3} \sum_{j=1}^N \sum_{\mathbf{n}} \frac{q_j \alpha^3 e^{-\alpha^2 |\mathbf{r} - (\mathbf{r}_j + \mathbf{n})|^2}}{\pi^{\frac{3}{2}}} e^{-i\mathbf{k}\cdot\mathbf{r}} d\mathbf{r} \\
&= \frac{1}{L^3} \int_{all\ space} \sum_{j=1}^N \frac{q_j \alpha^3 e^{-\alpha^2 |\mathbf{r} - \mathbf{r}_j|^2}}{\pi^{\frac{3}{2}}} e^{-i\mathbf{k}\cdot\mathbf{r}} d\mathbf{r} \\
&= \frac{1}{L^3} \sum_{j=1}^N q_j e^{-i\mathbf{k}\cdot\mathbf{r}_j} e^{\frac{-k^2}{4\alpha^2}}
\end{aligned} \tag{11}$$

The Fourier form of Poisson's equation ($-\nabla^2 \phi_1^{charge}(r) = 4\pi \rho_{G2}^{charge}(r)$ in standard form) applied to our situation is

$$k^2 \phi_1^{charge}(k) = 4\pi \hat{\rho}_{G2}^{charge}(k) \tag{12}$$

where $k = |\mathbf{k}|$ and $U_c^k = \frac{1}{2} \sum_{i=1}^N q_i \phi_1^{charge}(r)$ is the Fourier space contribution to the potential. Substituting (11) into (12) gives

$$\phi_1^{charge}(k) = \frac{4\pi}{k^2} \frac{1}{L^3} \sum_{j=1}^N q_j e^{-i\mathbf{k}\cdot\mathbf{r}_j} e^{\frac{-k^2}{4\alpha^2}} \tag{13}$$

which is only defined when $\mathbf{k} \neq \mathbf{0}$ because of the conditional convergence of the Ewald summation. However, ignoring the $\mathbf{k} = \mathbf{0}$ term is consistent with a periodic system with $\epsilon_s = \infty$ ^[12]. So, we shall ignore it as we are performing calculations as if the system had an infinite dielectric constant and then adding the correction term given in (6) to allow for a vacuum surround. Using (13) to compute $\phi_1^{charge}(r)$ gives

$$\begin{aligned}
\phi_1^{charge}(r) &= \sum_{\mathbf{k} \neq \mathbf{0}} \phi_1^{charge}(\mathbf{k}) e^{i\mathbf{k}\cdot\mathbf{r}} \\
&= \frac{1}{L^3} \sum_{\mathbf{k} \neq \mathbf{0}} \sum_{j=1}^N \frac{4\pi q_j}{k^2} e^{i\mathbf{k}\cdot(\mathbf{r} - \mathbf{r}_j)} e^{\frac{-k^2}{4\alpha^2}}.
\end{aligned}$$

So, we have

$$\begin{aligned}
U_c^k &= \frac{1}{2L^3} \sum_{i=1}^N q_i \sum_{\mathbf{k} \neq \mathbf{0}} \sum_{j=1}^N \frac{4\pi q_j}{k^2} e^{i\mathbf{k}\cdot(\mathbf{r}_i - \mathbf{r}_j)} e^{\frac{-k^2}{4\alpha^2}} \\
&= \frac{2\pi}{L^3} \sum_{\mathbf{k} \neq \mathbf{0}} \sum_{i=1}^N \sum_{j=1}^N \frac{q_i q_j}{k^2} e^{i\mathbf{k}\cdot\mathbf{r}_{ij}} e^{\frac{-k^2}{4\alpha^2}}.
\end{aligned} \tag{14}$$

In (14) we have the contribution from the second charge distribution (i.e. the reciprocal part of our potential energy equation). However, we can use the identity given in (4) to

rewrite it as

$$U_c^k = \frac{2\pi}{L^3} \sum_{\mathbf{k} \neq \mathbf{0}} \sum_{i=1}^N \sum_{j=1}^N \frac{q_i q_j}{k^2} e^{-\frac{k^2}{4\alpha^2}} \cos(\mathbf{k} \cdot \mathbf{r}_{ij}) \quad (15)$$

where we have ignored the imaginary sin term since we need to be able to perform computations in real space^[23]. Since the number of terms required in (15) increases as the Gaussian distribution gets wider it is important to balance the real space and reciprocal space sums to achieve optimal accuracy. Generally, α is set to be $\frac{5}{L}$ and 100-200 vectors \mathbf{k} are used^[1,23].

When introducing the cancelling distribution cloud described in (10) we included self-interaction terms, which we excluded from the real space sum using the \sum' notation. So, a further correction term is required to counteract this. The charge distribution that we have over counted by is

$$\rho_{G3}^{charge}(r) = \frac{q_i \alpha^3 e^{-\alpha^2 r^2}}{\pi^{\frac{3}{2}}}.$$

Using Poisson's equation as we did in the derivation of U_c^k we can work out the contribution of this to the overall potential. Using the spherical geometry of the cancelling charge cloud we can use Poisson's equation in the following form^[12]:

$$\begin{aligned} -\frac{1}{r} \frac{\partial^2 r \phi_2^{charge}(r)}{\partial r^2} &= 4\pi \rho_{G3}^{charge}(r) \\ \Rightarrow -\frac{\partial^2 r \phi_2^{charge}(r)}{\partial r^2} &= 4\pi r \rho_{G3}^{charge}(r) \end{aligned} \quad (16)$$

where $U_c^{self} = -\frac{1}{2} \sum_{i=1}^N q_i \phi_2^{charge}(r)$ is the self contribution to the potential. Partial integration of (16) gives

$$\begin{aligned} -\frac{\partial r \phi_2^{charge}(r)}{\partial r} &= \int_{\infty}^r 4\pi r \rho_{G3}^{charge}(r) dr \\ &= -\int_r^{\infty} \frac{2\pi q_i \alpha^3 e^{-\alpha^2 r^2}}{\pi^{\frac{3}{2}}} dr^2 \\ &= -\frac{2q_i \alpha e^{-\alpha^2 r^2}}{\sqrt{\pi}}. \end{aligned}$$

Performing a second partial integration gives

$$\begin{aligned} r \phi_2^{charge}(r) &= \int_0^r \frac{2q_i \alpha e^{-\alpha^2 r^2}}{\sqrt{\pi}} dr \\ &= q_i erf(\alpha r) \end{aligned}$$

where $erf(x) = \frac{2}{\sqrt{\pi}} \int_0^x e^{-t^2} dt$ is the Gauss error function related to the complementary error function used previously. The term we are trying to find occurs when $r = 0$. To

this end we have

$$\phi_2^{charge}(r=0) = \frac{2q_i\alpha}{\sqrt{\pi}}.$$

Hence the self contribution to the potential is given by^[12,23]

$$U_c^{self} = -\frac{\alpha}{\sqrt{\pi}} \sum_{i=1}^N q_i^2. \quad (17)$$

The same result can be obtained by using the Fourier space term given in (15) and setting $i = j$.

Combining the four terms; (6), (9), (15) and (17); discussed in this section gives the final expression

$$\begin{aligned} U_c(\epsilon_s = 1) &= U_c^r + U_c^k + U_c^{self} + U_c^{surf} \\ &= \sum_{i=1}^N \sum_{j=1}^N q_i q_j \left[\frac{1}{2} \left(\sum_{\mathbf{n} \in \mathbb{Z}^3} \frac{erfc(\alpha|\mathbf{r}_{ij} + \mathbf{n}|)}{|\mathbf{r}_{ij} + \mathbf{n}|} \right) + \frac{2\pi}{L^3} \sum_{\mathbf{k} \neq \mathbf{0}} \frac{1}{k^2} e^{-\frac{k^2}{4\alpha^2}} \cos(\mathbf{k} \cdot \mathbf{r}_{ij}) \right] \\ &\quad - \frac{\alpha}{\sqrt{\pi}} \sum_{i=1}^N q_i^2 + \frac{2\pi}{3L^3} \left| \sum_{i=1}^N q_i \mathbf{r}_i \right|^2 \end{aligned} \quad (18)$$

for the Ewald summation of the potential energy of charge-charge interactions.

3.1.2 Dipole-Dipole Interactions

The original Ewald method described in §3.1.1 is easily extended to dipolar systems by simply replacing q_i by $\boldsymbol{\mu}_i \cdot \nabla_{\mathbf{r}_i}$, where $\boldsymbol{\mu}_i$ is a dipole, in the derivation of (18). The detailed derivations given by De Leeuw et al.^[11] include the Ewald method for dipole-dipole interactions but again the details are not repeated here.

The total paired potential energy of dipole-dipole interactions in a three dimensional periodic system is given by⁴

$$U_d = \frac{1}{2} \sum_{\mathbf{n}} \left(\sum_{i=1}^N \sum_{j=1}^N \frac{\boldsymbol{\mu}_i \cdot \boldsymbol{\mu}_j}{|\mathbf{r}_{ij} + \mathbf{n}|^3} - \frac{3[\boldsymbol{\mu}_i \cdot (\mathbf{r}_{ij} + \mathbf{n})][\boldsymbol{\mu}_j \cdot (\mathbf{r}_{ij} + \mathbf{n})]}{|\mathbf{r}_{ij} + \mathbf{n}|^5} \right) \quad (19)$$

where $\boldsymbol{\mu}_i$ and $\boldsymbol{\mu}_j$ are two dipoles and the subscript d denotes that this is the derivation for dipole-dipole interactions. The rest of the components are as defined in §3.1.1 (see Appendix A)^[33].

The simulation boxes are to be summed by building up in the spherical manner described in Figure 4 as we did for charge-charge interactions. Also, as discussed in §3.1.1 a surface term is required in order to satisfy the relationship between the dielectric constants $\epsilon_s = \infty$ and $\epsilon_s = 1$. In the case of dipole-dipole interactions the surface contribution for

⁴Remember that we are omitting all factors of $4\pi\epsilon_0$.

a system surrounded by a vacuum is^[1,33]

$$U_d^{surf} = \frac{2\pi}{3L^3} \sum_{i=1}^N \sum_{j=1}^N \boldsymbol{\mu}_i \cdot \boldsymbol{\mu}_j. \quad (20)$$

Combining the slow converging summation in (19) with a suitable neutralising Gaussian distribution we get the following real space contribution to our potential^[1,33]:

$$U_d^r = \frac{1}{2} \sum_{\mathbf{n} \in \mathbb{Z}^3} \sum_{i=1}^N \sum_{j=1}^N [(\boldsymbol{\mu}_i \cdot \boldsymbol{\mu}_j)B(|\mathbf{r}_{ij} + \mathbf{n}|) - (\boldsymbol{\mu}_i \cdot (\mathbf{r}_{ij} + \mathbf{n}))(\boldsymbol{\mu}_j \cdot (\mathbf{r}_{ij} + \mathbf{n}))C(|\mathbf{r}_{ij} + \mathbf{n}|)] \quad (21)$$

where the two components B and C are given by

$$B(r) = \frac{\operatorname{erfc}(\alpha r) + \left(\frac{2\alpha r}{\sqrt{\pi}}\right) \exp(-\alpha^2 r^2)}{r^3},$$

$$C(r) = \frac{3 \operatorname{erfc}(\alpha r) + \left(\frac{2\alpha r}{\sqrt{\pi}}\right)(3 + 2\alpha^2 r^2) \exp(-\alpha^2 r^2)}{r^5}.$$

As before we get the Fourier contribution to the potential by introducing another Gaussian distribution to negate the effects of the one added previously and taking the Fourier transform. This gives the final result^[1,33]

$$U_d^k = \frac{2\pi}{L^3} \sum_{\substack{\mathbf{k} \in \mathbb{Z}^3 \\ \mathbf{k} \neq \mathbf{0}}} \sum_{i=1}^N \sum_{j=1}^N \frac{1}{k^2} (\boldsymbol{\mu}_i \cdot \mathbf{k})(\boldsymbol{\mu}_j \cdot \mathbf{k}) e^{\frac{-k^2}{4\alpha^2}} \cos(\mathbf{k} \cdot \mathbf{r}_{ij}). \quad (22)$$

Finally, a further term is introduced and manipulated to subtract the self-interactions that were introduced by the second, cancelling, Gaussian distribution. Once this has been done we get the following correction term^[1,33]:

$$U_d^{self} = - \sum_{i=1}^N \frac{2\alpha^3 \mu_i^2}{3\sqrt{\pi}}. \quad (23)$$

Combining the four components; (20), (21), (22) and (23); gives the final expression for the Ewald summation of the potential energy of dipole-dipole interactions (24)^[1]. At a glance it is obvious that this is much more complicated than the corresponding formula for charge-charge interactions, which is one reason early simulations of dipolar interactions did not make use of Ewald summations.⁵

⁵Again all factors of $4\pi\epsilon_0$ have been omitted.

$$\begin{aligned}
U_d(\epsilon_s = 1) &= U_d^r + U_d^k + U_d^{self} + U_d^{surf} \\
&= \sum_{i=1}^N \sum_{j=1}^N \left[\frac{1}{2} \sum_{\mathbf{n} \in \mathbb{Z}^3} ' [(\boldsymbol{\mu}_i \cdot \boldsymbol{\mu}_j) B(|\mathbf{r}_{ij} + \mathbf{n}|) - (\boldsymbol{\mu}_i \cdot (\mathbf{r}_{ij} + \mathbf{n})) (\boldsymbol{\mu}_j \cdot (\mathbf{r}_{ij} + \mathbf{n})) C(|\mathbf{r}_{ij} + \mathbf{n}|)] \right. \\
&\quad \left. + \frac{2\pi}{L^3} \sum_{\mathbf{k} \in \mathbb{Z}^3, \mathbf{k} \neq \mathbf{0}} \frac{1}{k^2} (\boldsymbol{\mu}_i \cdot \mathbf{k}) (\boldsymbol{\mu}_j \cdot \mathbf{k}) e^{\frac{-k^2}{4\alpha^2}} \cos(\mathbf{k} \cdot \mathbf{r}_{ij}) \right] \\
&\quad - \sum_{i=1}^N \frac{2\alpha^3 \mu_i^2}{3\sqrt{\pi}} + \frac{2\pi}{3L^3} \sum_{i=1}^N \sum_{j=1}^N \boldsymbol{\mu}_i \cdot \boldsymbol{\mu}_j
\end{aligned} \tag{24}$$

with

$$\begin{aligned}
B(r) &= \frac{\operatorname{erfc}(\alpha r) + \left(\frac{2\alpha r}{\sqrt{\pi}}\right) e^{-\alpha^2 r^2}}{r^3}, \\
C(r) &= \frac{3 \operatorname{erfc}(\alpha r) + \left(\frac{2\alpha r}{\sqrt{\pi}}\right) (3 + 2\alpha^2 r^2) e^{-\alpha^2 r^2}}{r^5}.
\end{aligned}$$

3.1.3 Fast Fourier Transforms

In §3.1.1 (and §3.1.2) we make use of Fourier transforms. The computing time required for the Ewald summation can be greatly reduced by using fast Fourier transforms (FFTs), a technique introduced in 1965, instead. There are many different variations of the FFT but they all make use of the ideas detailed in this section. The account of the method for the one dimensional case given here closely follows that provided by Gibbs^[14]. It can easily be extended to three dimensional space for our problem by replacing the product rk that arises with the dot product $\mathbf{r} \cdot \mathbf{k}$. Bracewell^[3] gives two alternative ways of approaching the derivation of the FFT as well as discussing practical implications surrounding its application.

To begin with we take an infinite series of Dirac delta functions, that are zero everywhere except at the point $n\Delta r$ and multiply the function $f(r)$ by this series^[14].

$$\begin{aligned}
\delta_1(r) &= \sum_{n=-\infty}^{\infty} \delta(r - n\Delta r) \\
\Rightarrow \delta_1(r)f(r) &= \sum_{n=-\infty}^{\infty} \delta(r - n\Delta r)f(r) \\
&= \sum_{n=-\infty}^{\infty} f(n\Delta r)
\end{aligned} \tag{25}$$

Taking the Fourier transform of (25) and integrating gives

$$\widehat{\delta_1 f}(\xi) = \sum_{n=-\infty}^{\infty} f(n\Delta r) e^{-2i\pi\xi n\Delta r} \quad (26)$$

for some $\xi \in \mathbb{R}$. We can truncate the sum in (26) by assuming that $f(r) = 0$ unless $0 \leq n < M$ for a sufficiently large M so that

$$\widehat{\delta_1 f}(\xi) = \sum_{n=0}^{M-1} f(n\Delta r) e^{-2i\pi\xi n\Delta r}.$$

This equation now contains M pieces of information that need to be evaluated at points $\xi = \frac{k}{M\Delta r}$ for $k = 0, \dots, M$ ^[14]. So, the discrete Fourier transform (DFT) is taken to be

$$F(k) = \widehat{\delta_1 f} \left(\frac{k}{M\Delta r} \right) = \sum_{n=0}^{M-1} f(n\Delta r) e^{-\frac{2i\pi nk}{M}}. \quad (27)$$

However, in (27) many values are calculated twice and it is by preventing this that the FFT makes computation quicker. If we take M to be even we can split the sum in (27) into its even and odd components as shown below.

$$\begin{aligned} F(k) &= F_{\text{even}}(k) + F_{\text{odd}}(k) \\ &= \sum_{n=0}^{\frac{M}{2}-1} f((2n)\Delta r) e^{-\frac{2i\pi(2n)k}{M}} + \sum_{n=0}^{\frac{M}{2}-1} f((2n+1)\Delta r) e^{-\frac{2i\pi(2n+1)k}{M}} \end{aligned} \quad (28)$$

Using the results in (28) we can derive an equation for $F\left(k + \frac{M}{2}\right)$.

$$\begin{aligned} F\left(k + \frac{M}{2}\right) &= \sum_{n=0}^{\frac{M}{2}-1} f((2n)\Delta r) e^{-\frac{2i\pi(2n)\left(k + \frac{M}{2}\right)}{M}} + \sum_{n=0}^{\frac{M}{2}-1} f((2n+1)\Delta r) e^{-\frac{2i\pi(2n+1)\left(k + \frac{M}{2}\right)}{M}} \\ &= \sum_{n=0}^{\frac{M}{2}-1} f((2n)\Delta r) e^{-\frac{2i\pi(2n)k}{M}} e^{-i\pi(2n)} + \sum_{n=0}^{\frac{M}{2}-1} f((2n+1)\Delta r) e^{-\frac{2i\pi(2n+1)k}{M}} e^{-i\pi(2n+1)} \end{aligned} \quad (29)$$

However, using the identity stated in (4) we have the following results

$$\begin{aligned} e^{-i\pi(2n)} &= \cos(-\pi(2n)) + i \sin(-\pi(2n)) \\ &= 1 + 0 = 1, \end{aligned}$$

and

$$\begin{aligned} e^{-i\pi(2n+1)} &= \cos(-\pi(2n+1)) + i \sin(-\pi(2n+1)) \\ &= -1 + 0 = -1. \end{aligned}$$

So, (29) becomes

$$\begin{aligned} F\left(k + \frac{M}{2}\right) &= \sum_{n=0}^{\frac{M}{2}-1} f((2n)\Delta r) e^{-\frac{2i\pi(2n)k}{M}} - \sum_{n=0}^{\frac{M}{2}-1} f((2n+1)\Delta r) e^{-\frac{2i\pi(2n+1)k}{M}} \\ &= F_{\text{even}}(k) - F_{\text{odd}}(k). \end{aligned} \quad (30)$$

It is the relationship between $F(k)$ and $F\left(k + \frac{M}{2}\right)$ given in (30) that the FFT uses to avoid having as many calculations to perform as would be required in an ordinary Fourier transform. Press et al.^[29] recognise the particular advantage of using the above technique recursively to further enhance computational ability and go into great detail regarding the implementation of this.

An advanced adaptation of the FFT method called the FFTW (fastest Fourier transform in the West) chooses from several variants of the method in order to reduce the computing time to $\mathcal{O}(N \log N)$ ^[13]. It is the fastest free software that implements the FFT.

3.2 Application of Ewald Summations

From this point forward we assume that the dielectric constant is $\epsilon_s = 1$, as in previous calculations, so we will not continue to carry this parameter forward explicitly in the notation used. This section is only concerned with the application of dipole-dipole interactions and so we consider only the formulae derived in §3.1.2. To avoid complicating the notation here we will drop the subscript d when discussing individual components and replace U_d with U since we know that all calculations relate to dipoles.

In order to program, and hence apply, the Ewald summation given in (24) we need to truncate the two infinite sums contained within. This is done by choosing a cut-off in real space, r_c , at which to end the sum in (21) and a cut-off in reciprocal space, k_c , at which to end the sum in (22). If $r_c \leq \frac{L}{2}$ then the real space sum reduces to the standard minimum image convention^[33] (i.e. each particle only interacts with the closest image of the other particles in the system). Truncating the summations introduces errors as discussed in §3.3.

When the formulae for dipolar interactions were derived the results of all summations were halved. This is because the way that the equations were written meant that each interaction was counted twice; i.e. particle i interacting with particle j was counted as well

as particle j interacting with particle i when in fact these are the same thing. An alternative way to avoid this would be to write the double summation as $\sum_{i=1}^{N-1} \sum_{j=i+1}^N$ instead (meaning the factor of $\frac{1}{2}$ is not needed). This approach is favoured when programming since it means less calculations are performed, saving valuable computing effort.

Newton's third law of motion is stated in the box below, where \mathbf{F} represents force, $\boldsymbol{\tau}$ is torque and the subscript ij means that particle i is influencing particle j :

For every action there is an equal and opposite reaction ($\mathbf{F}_{ij} = -\mathbf{F}_{ji}$ and $\boldsymbol{\tau}_{ij} = -\boldsymbol{\tau}_{ji}$).

This means that if we know the force or torque of particle i acting on particle j then we also know the effect particle j has on particle i . This relationship can be used to reduce the number of calculations required and provide another way of cutting computational time in simulations.

3.2.1 Force

Hinchliffe^[17] provides the following account for the relationship between the potential energy, U , and force. An expression for the total energy of a system is given by

$$E = \frac{1}{2}m(\mathbf{v} \cdot \mathbf{v}) + U \quad (31)$$

where $\frac{1}{2}m(\mathbf{v} \cdot \mathbf{v})$ is the kinetic energy given mass, m , and velocity, \mathbf{v} . Differentiating (31) with respect to time gives

$$\begin{aligned} \frac{dE}{dt} &= m \left(\mathbf{v} \cdot \frac{d\mathbf{v}}{dt} \right) + \frac{dU}{dt} \\ \Rightarrow \frac{dE}{dt} &= m \left(\mathbf{v} \cdot \frac{d\mathbf{v}}{dt} \right) + \frac{dU}{d\mathbf{r}} \cdot \frac{d\mathbf{r}}{dt} \end{aligned}$$

by the chain rule. As the energy, E , is constant in time (since we are dealing with a closed system, i.e. a microcanonical ensemble (NVE)) its first derivative will be zero and $\mathbf{v} = \frac{d\mathbf{r}}{dt}$ which leads to the following:

$$0 = \left(m \frac{d^2\mathbf{r}}{dt^2} + \frac{dU}{d\mathbf{r}} \right) \cdot \frac{d\mathbf{r}}{dt}.$$

Since we know that the velocity is not zero the contents of the brackets must either be zero or orthogonal to the velocity. Furthermore, using Newton's second law of motion (stated in §2) we know that the first term in the brackets is mass \times acceleration and thus, is force. So, finally we have the relationship

$$\mathbf{F} = -\nabla(U).$$

Hence, in order to find the force, \mathbf{F}_i , acting on a particular particle, i , we need to take U for that particle and differentiate with respect to \mathbf{r}_i .

Due to the complexity of the equation it is easier to tackle this task component by component; i.e. $\mathbf{F}_i = -\frac{\partial(U_i)}{\partial\mathbf{r}_i} = -\frac{\partial(U_i^r)}{\partial\mathbf{r}_i} - \frac{\partial(U_i^k)}{\partial\mathbf{r}_i} - \frac{\partial(U_i^{self})}{\partial\mathbf{r}_i} - \frac{\partial(U_i^{surf})}{\partial\mathbf{r}_i}$. Clearly there is no contribution from the U^{self} and U^{surf} terms since there is no dependence on \mathbf{r}_i in either. Physically, this means that particles do not exert any force on themselves and there is no effect from forces outside of the system. So, from (21) we get

$$\begin{aligned}\mathbf{F}_i^r &= -\frac{\partial(U_i^r)}{\partial\mathbf{r}_i} \\ &= -\sum_{j=1}^N \sum_{\mathbf{n} \in \mathbb{Z}^3} \left\{ (\boldsymbol{\mu}_i \cdot \boldsymbol{\mu}_j) \frac{\partial}{\partial\mathbf{r}_i} B(|\mathbf{r}_{ij} + \mathbf{n}|) \right. \\ &\quad \left. - \frac{\partial}{\partial\mathbf{r}_i} [\boldsymbol{\mu}_i \cdot (\mathbf{r}_{ij} + \mathbf{n})][\boldsymbol{\mu}_j \cdot (\mathbf{r}_{ij} + \mathbf{n})] C(|\mathbf{r}_{ij} + \mathbf{n}|) \right\}. \quad (32)\end{aligned}$$

Differentiating $B(r)$ and $C(r)$ (remembering that $r = |\mathbf{r}_{ij} + \mathbf{n}|$ and $\mathbf{r}_{ij} = \mathbf{r}_i - \mathbf{r}_j$) gives

$$\begin{aligned}\frac{\partial B}{\partial r} &= \frac{r^3 \left[-\frac{2\alpha}{\sqrt{\pi}} e^{-\alpha^2 r^2} + \frac{2\alpha}{\sqrt{\pi}} e^{-\alpha^2 r^2} - 2\alpha^2 r \left(\frac{2\alpha r}{\sqrt{\pi}} \right) e^{-\alpha^2 r^2} \right] - 3r^2 \left[\operatorname{erfc}(\alpha r) + \frac{2\alpha r}{\sqrt{\pi}} e^{-\alpha^2 r^2} \right]}{r^6} \\ &= \frac{-\frac{4\alpha^3 r^3}{\sqrt{\pi}} e^{-\alpha^2 r^2} - 3\operatorname{erfc}(\alpha r) - \frac{6\alpha r}{\sqrt{\pi}} e^{-\alpha^2 r^2}}{r^4} \\ &= -(|\mathbf{r}_{ij} + \mathbf{n}|) C(r)\end{aligned}$$

and

$$\begin{aligned}\frac{\partial C}{\partial r} &= \frac{r^5 \left[-\frac{6\alpha}{\sqrt{\pi}} e^{-\alpha^2 r^2} + \frac{6\alpha}{\sqrt{\pi}} e^{-\alpha^2 r^2} - 2\alpha^2 r \left(\frac{6\alpha r}{\sqrt{\pi}} \right) e^{-\alpha^2 r^2} + \frac{12\alpha^3 r^2}{\sqrt{\pi}} e^{-\alpha^2 r^2} - 2\alpha^2 r \left(\frac{4\alpha^3 r^3}{\sqrt{\pi}} \right) e^{-\alpha^2 r^2} \right]}{r^{10}} \\ &\quad - \frac{5r^4 \left[3\operatorname{erfc}(\alpha r) + \frac{6\alpha r}{\sqrt{\pi}} e^{-\alpha^2 r^2} + \frac{4\alpha^3 r^3}{\sqrt{\pi}} e^{-\alpha^2 r^2} \right]}{r^{10}} \\ &= \frac{-\frac{8\alpha^5 r^5}{\sqrt{\pi}} e^{-\alpha^2 r^2} - 15\operatorname{erfc}(\alpha r) - \frac{30\alpha r}{\sqrt{\pi}} e^{-\alpha^2 r^2} - \frac{20\alpha^3 r^3}{\sqrt{\pi}} e^{-\alpha^2 r^2}}{r^6} \\ &= -(|\mathbf{r}_{ij} + \mathbf{n}|) D(r)\end{aligned}$$

where

$$D(r) = \frac{15\operatorname{erfc}(\alpha r) + \left(\frac{2\alpha r}{\sqrt{\pi}} \right) (15 + 10\alpha^2 r^2 + 4\alpha^4 r^4) e^{-\alpha^2 r^2}}{r^7}.$$

Using the results given above we can now perform the required differentiation in (32) as

follows:

$$\begin{aligned}
\mathbf{F}_i^r &= \sum_{j=1}^N \sum_{\mathbf{n} \in \mathbb{Z}^3} \left\{ (\boldsymbol{\mu}_i \cdot \boldsymbol{\mu}_j) [(\mathbf{r}_{ij} + \mathbf{n})C(|\mathbf{r}_{ij} + \mathbf{n}|) - B] \right. \\
&\quad + C(|\mathbf{r}_{ij} + \mathbf{n}|)(\boldsymbol{\mu}_j[\boldsymbol{\mu}_i \cdot (\mathbf{r}_{ij} + \mathbf{n})] + \boldsymbol{\mu}_i[\boldsymbol{\mu}_j \cdot (\mathbf{r}_{ij} + \mathbf{n})]) \\
&\quad \left. + [\boldsymbol{\mu}_i \cdot (\mathbf{r}_{ij} + \mathbf{n})][\boldsymbol{\mu}_j \cdot (\mathbf{r}_{ij} + \mathbf{n})][C - (\mathbf{r}_{ij} + \mathbf{n})D(|\mathbf{r}_{ij} + \mathbf{n}|)] \right\} \\
&= \sum_{j=1}^N \sum_{\mathbf{n} \in \mathbb{Z}^3} \left\{ \{(\boldsymbol{\mu}_i \cdot \boldsymbol{\mu}_j)(\mathbf{r}_{ij} + \mathbf{n}) + \boldsymbol{\mu}_j[\boldsymbol{\mu}_i \cdot (\mathbf{r}_{ij} + \mathbf{n})] + \boldsymbol{\mu}_i[\boldsymbol{\mu}_j \cdot (\mathbf{r}_{ij} + \mathbf{n})]\}C(|\mathbf{r}_{ij} + \mathbf{n}|) \right. \\
&\quad \left. - [\boldsymbol{\mu}_i \cdot (\mathbf{r}_{ij} + \mathbf{n})][\boldsymbol{\mu}_j \cdot (\mathbf{r}_{ij} + \mathbf{n})](\mathbf{r}_{ij} + \mathbf{n})D(|\mathbf{r}_{ij} + \mathbf{n}|) \right\} \quad (33)
\end{aligned}$$

since we can eliminate the scalar terms. Notice that we were able to ignore the modulus signs when differentiating as a result of the periodicity of the system. Similarly, using (22) we get

$$\begin{aligned}
\mathbf{F}_i^k &= -\frac{\partial(U_i^k)}{\partial \mathbf{r}_i} \\
&= -\frac{4\pi}{L^3} \sum_{j=1}^N \sum_{\substack{\mathbf{k} \in \mathbb{Z}^3 \\ \mathbf{k} \neq \mathbf{0}}} \frac{1}{k^2} e^{-\left(\frac{\pi \mathbf{k}}{\alpha L}\right)^2} (\boldsymbol{\mu}_i \cdot \mathbf{k})(\boldsymbol{\mu}_j \cdot \mathbf{k}) \frac{\partial}{\partial \mathbf{r}_i} \cos(\mathbf{k} \cdot \mathbf{r}_{ij}) \\
&= \frac{4\pi}{L^3} \sum_{j=1}^N \sum_{\substack{\mathbf{k} \in \mathbb{Z}^3 \\ \mathbf{k} \neq \mathbf{0}}} \frac{\mathbf{k}}{k^2} e^{-\left(\frac{\pi \mathbf{k}}{\alpha L}\right)^2} (\boldsymbol{\mu}_i \cdot \mathbf{k})(\boldsymbol{\mu}_j \cdot \mathbf{k}) \sin(\mathbf{k} \cdot \mathbf{r}_{ij}). \quad (34)
\end{aligned}$$

Combining (33) and (34) gives the total force calculation

$$\begin{aligned}
\mathbf{F}_i &= \sum_{j=1}^N \left\{ \sum_{\mathbf{n} \in \mathbb{Z}^3} \left\{ \{(\boldsymbol{\mu}_i \cdot \boldsymbol{\mu}_j)(\mathbf{r}_{ij} + \mathbf{n}) + \boldsymbol{\mu}_j[\boldsymbol{\mu}_i \cdot (\mathbf{r}_{ij} + \mathbf{n})] + \boldsymbol{\mu}_i[\boldsymbol{\mu}_j \cdot (\mathbf{r}_{ij} + \mathbf{n})]\}C(|\mathbf{r}_{ij} + \mathbf{n}|) \right. \right. \\
&\quad \left. \left. - [\boldsymbol{\mu}_i \cdot (\mathbf{r}_{ij} + \mathbf{n})][\boldsymbol{\mu}_j \cdot (\mathbf{r}_{ij} + \mathbf{n})](\mathbf{r}_{ij} + \mathbf{n})D(|\mathbf{r}_{ij} + \mathbf{n}|) \right\} \right. \\
&\quad \left. + \frac{4\pi}{L^3} \sum_{\substack{\mathbf{k} \in \mathbb{Z}^3 \\ \mathbf{k} \neq \mathbf{0}}} \frac{\mathbf{k}}{k^2} e^{-\left(\frac{\pi \mathbf{k}}{\alpha L}\right)^2} (\boldsymbol{\mu}_i \cdot \mathbf{k})(\boldsymbol{\mu}_j \cdot \mathbf{k}) \sin(\mathbf{k} \cdot \mathbf{r}_{ij}) \right\}.
\end{aligned}$$

3.2.2 Torque

Torque is an important factor in the behaviour of dipoles, particularly when considering magnetic fluids, as the particles have a tendency to orientate themselves in the direction of the external field being applied. This is one of the behaviours noticed when simulating the formation of the chain structures discussed in §1.

The torque, $\boldsymbol{\tau}_i$, of a particle, i , is calculated using the electrostatic field, \mathbf{E}_i , at the

position of i using the following relationship

$$\boldsymbol{\tau}_i = \boldsymbol{\mu}_i \times \mathbf{E}_i$$

where $\mathbf{E}_i = -\frac{\partial(U_i)}{\partial\boldsymbol{\mu}_i}$. As with force we will calculate the torque one component at a time. Clearly there is again no contribution from the self term. So, calculating the torque contribution in real space for a particular i yields

$$\begin{aligned} \mathbf{E}_i^r &= -\frac{\partial(U_i^r)}{\partial\boldsymbol{\mu}_i} \\ &= -\sum_{\mathbf{n} \in \mathbb{Z}^3} \prime \sum_{j=1}^N \frac{\partial}{\partial\boldsymbol{\mu}_i} [(\boldsymbol{\mu}_i \cdot \boldsymbol{\mu}_j)B(|\mathbf{r}_{ij} + \mathbf{n}|) - (\boldsymbol{\mu}_i \cdot (\mathbf{r}_{ij} + \mathbf{n}))(\boldsymbol{\mu}_j \cdot (\mathbf{r}_{ij} + \mathbf{n}))C(|\mathbf{r}_{ij} + \mathbf{n}|)] \\ &= -\sum_{\mathbf{n} \in \mathbb{Z}^3} \prime \sum_{j=1}^N [\boldsymbol{\mu}_j B(|\mathbf{r}_{ij} + \mathbf{n}|) - (\mathbf{r}_{ij} + \mathbf{n})(\boldsymbol{\mu}_j \cdot (\mathbf{r}_{ij} + \mathbf{n}))C(|\mathbf{r}_{ij} + \mathbf{n}|)] \\ \Rightarrow \boldsymbol{\tau}_i^r &= -\sum_{\mathbf{n} \in \mathbb{Z}^3} \prime \sum_{j=1}^N [(\boldsymbol{\mu}_i \times \boldsymbol{\mu}_j)B(|\mathbf{r}_{ij} + \mathbf{n}|) - \boldsymbol{\mu}_i \times (\mathbf{r}_{ij} + \mathbf{n})(\boldsymbol{\mu}_j \cdot (\mathbf{r}_{ij} + \mathbf{n}))C(|\mathbf{r}_{ij} + \mathbf{n}|)]. \end{aligned} \quad (35)$$

Similarly, the Fourier space contribution is given by

$$\begin{aligned} \mathbf{E}_i^k &= -\frac{\partial(U_i^k)}{\partial\boldsymbol{\mu}_i} \\ &= -\frac{4\pi}{L^3} \sum_{\substack{\mathbf{k} \in \mathbb{Z}^3 \\ \mathbf{k} \neq \mathbf{0}}} \sum_{j=1}^N \frac{1}{k^2} e^{(\frac{-\pi\mathbf{k}}{\alpha L})^2} \cos(\mathbf{k} \cdot \mathbf{r}_{ij}) \frac{\partial}{\partial\boldsymbol{\mu}_i} [(\boldsymbol{\mu}_i \cdot \mathbf{k})(\boldsymbol{\mu}_j \cdot \mathbf{k})] \\ &= -\frac{4\pi}{L^3} \sum_{\substack{\mathbf{k} \in \mathbb{Z}^3 \\ \mathbf{k} \neq \mathbf{0}}} \sum_{j=1}^N \frac{1}{k^2} \mathbf{k}(\boldsymbol{\mu}_j \cdot \mathbf{k}) e^{(\frac{-\pi\mathbf{k}}{\alpha L})^2} \cos(\mathbf{k} \cdot \mathbf{r}_{ij}) \\ \Rightarrow \boldsymbol{\tau}_i^k &= -\frac{4\pi}{L^3} \sum_{\substack{\mathbf{k} \in \mathbb{Z}^3 \\ \mathbf{k} \neq \mathbf{0}}} \sum_{j=1}^N \frac{1}{k^2} (\boldsymbol{\mu}_i \times \mathbf{k})(\boldsymbol{\mu}_j \cdot \mathbf{k}) e^{(\frac{-\pi\mathbf{k}}{\alpha L})^2} \cos(\mathbf{k} \cdot \mathbf{r}_{ij}). \end{aligned} \quad (36)$$

Finally the surface term contribution is

$$\begin{aligned}
\mathbf{E}_i^{surf} &= -\frac{\partial(U_i^{surf})}{\partial\boldsymbol{\mu}_i} \\
&= -\frac{4\pi}{3L^3} \sum_{j=1}^N \frac{\partial}{\partial\boldsymbol{\mu}_i} \boldsymbol{\mu}_i \cdot \boldsymbol{\mu}_j \\
&= -\frac{4\pi}{3L^3} \sum_{j=1}^N \boldsymbol{\mu}_j \\
\boldsymbol{\tau}_i^{surf} &= -\frac{4\pi}{3L^3} \sum_{j=1}^N \boldsymbol{\mu}_i \times \boldsymbol{\mu}_j.
\end{aligned} \tag{37}$$

Combining the three terms; (35), (36) and (37); to obtain the overall torque we get

$$\begin{aligned}
\boldsymbol{\tau}_i &= \boldsymbol{\tau}_i^r + \boldsymbol{\tau}_i^k + \boldsymbol{\tau}_i^{surf} \\
&= -\sum_{j=1}^N \left\{ \sum_{\substack{\mathbf{n} \in \mathbb{Z}^3 \\ \mathbf{n} \neq \mathbf{0}}} \left[(\boldsymbol{\mu}_i \times \boldsymbol{\mu}_j) B(|\mathbf{r}_{ij} + \mathbf{n}|) - \boldsymbol{\mu}_i \times (\mathbf{r}_{ij} + \mathbf{n}) (\boldsymbol{\mu}_j \cdot (\mathbf{r}_{ij} + \mathbf{n})) C(|\mathbf{r}_{ij} + \mathbf{n}|) \right] \right. \\
&\quad \left. + \frac{4\pi}{L^3} \left[\sum_{\substack{\mathbf{k} \in \mathbb{Z}^3 \\ \mathbf{k} \neq \mathbf{0}}} \frac{1}{k^2} (\boldsymbol{\mu}_i \times \mathbf{k}) (\boldsymbol{\mu}_j \cdot \mathbf{k}) e^{\left(\frac{-\pi k}{\alpha L}\right)^2} \cos(\mathbf{k} \cdot \mathbf{r}_{ij}) + \frac{1}{3} \sum_{j=1}^N \boldsymbol{\mu}_i \times \boldsymbol{\mu}_j \right] \right\}.
\end{aligned}$$

3.3 Errors in Ewald Summations

As with the previous section we are only concerned with dipolar interactions, since these are the ones present in magnetic fluids. As such we will again omit the subscript d when discussing various elements in order to keep notation simple.

Wang and Holm^[33] derived and successfully tested estimates for the errors in the Ewald summation derived for dipoles in §3.1.2 and also the forces and torques given in §3.2. All of the equations and results discussed in this section are taken from their work.

As described in §3.2 there are two cut-offs; one in real space, r_c , and one in reciprocal space, k_c . So, there are errors in real space and reciprocal space, which we assume to be independent of each other. There are no errors in the surface or self terms since there are no truncations in these. Due to the assumption of independence of errors we can write the total cut-off error for the Ewald summation as

$$\Delta\Theta = \sqrt{(\Delta\Theta^r)^2 + (\Delta\Theta^k)^2}$$

where Θ represents U , F and τ .

In molecular dynamics accuracy is generally tested using the root mean square (rms)

error in the forces:

$$\Delta F = \sqrt{\frac{1}{N} \sum_{i=1}^N (\Delta \mathbf{F}_i)^2} = \sqrt{\frac{1}{N} \sum_{i=1}^N (\mathbf{F}_i - \mathbf{F}_i^{exact})^2} \quad (38)$$

where \mathbf{F}_i is the force on particle i calculated by the Ewald summation and \mathbf{F}_i^{exact} is the exact force on that particle. This method will be employed throughout this section, although clearly our results will all be approximations since we do not know what the exact force is.

The error estimates can be used to look at the three key parameters; r_c , k_c and α ; with the aim of balancing them to achieve the highest possible accuracy without compromising efficiency. This is discussed further in §3.3.3.

3.3.1 Errors in Real Space

The error in \mathbf{F}_i^r comes from the $N - 1$ interactions of particle i with all of the other dipoles in the system and each contribution to the error must be proportional to the two dipoles involved. Hence we define the real space cut-off error in the force to be

$$\Delta \mathbf{F}_i^r = |\boldsymbol{\mu}_i| \sum_{\substack{j=1 \\ j \neq i}}^N |\boldsymbol{\mu}_j| \boldsymbol{\chi}_{ij}^r. \quad (39)$$

The vector $\boldsymbol{\chi}_{ij}^r$ uses the orientations and separation distance of two dipoles to ascertain the direction and magnitude of their interaction's contribution to the error. By performing the dot products in the real space force term given by (33) we can see that $\boldsymbol{\chi}_{ij}^r$ is defined as follows:

$$\boldsymbol{\chi}_{ij}^r = \sum_{\substack{\mathbf{r} \\ r > r_c}} \left\{ [\hat{\mathbf{r}} \cos \omega(\hat{\boldsymbol{\mu}}_i, \hat{\boldsymbol{\mu}}_j) + \hat{\boldsymbol{\mu}}_i \cos \omega(\hat{\boldsymbol{\mu}}_j, \hat{\mathbf{r}}) + \hat{\boldsymbol{\mu}}_j \cos \omega(\hat{\boldsymbol{\mu}}_i, \hat{\mathbf{r}})] r C(r) \right. \\ \left. - \hat{\mathbf{r}} \cos \omega(\hat{\boldsymbol{\mu}}_i, \hat{\mathbf{r}}) \cos \omega(\hat{\boldsymbol{\mu}}_j, \hat{\mathbf{r}}) r^3 D(r) \right\} \quad (40)$$

where $\hat{\boldsymbol{\mu}}_i$ and $\hat{\boldsymbol{\mu}}_j$ are unit vectors along the orientation of dipoles i and j , $\hat{\mathbf{r}}$ is a unit vector along $\mathbf{r} = \mathbf{r}_{ij} + \mathbf{n}$ and $\omega(\mathbf{a}, \mathbf{b})$ denotes the angle between vectors \mathbf{a} and \mathbf{b} .

Although it is not true for all dipolar systems, it is a reasonable starting point to assume that the positions and orientations of dipoles beyond our cut-off are random and hence, that their contributions to the error are uncorrelated. Based on this assumption the average error contribution over all configurations of particles is given by

$$\langle \boldsymbol{\chi}_{ij}^r \cdot \boldsymbol{\chi}_{im}^r \rangle = \delta_{jm} \langle (\boldsymbol{\chi}_{ij}^r)^2 \rangle = \delta_{jm} (\chi^r)^2 \quad (41)$$

where δ_{jm} is the Kronecker delta function, which equals one if $j = m$ and zero otherwise. The change of notation in (41) comes about because the mean square force error for two dipoles, $\langle(\boldsymbol{\chi}_{ij}^r)^2\rangle$, is no longer dependent on i and j .

Combining the results in (39) and (41) we look at the average over all particle configurations of the squared real space error:

$$\begin{aligned}\langle(\Delta\mathbf{F}_i^r)^2\rangle &= \mu_i^2 \sum_{j \neq i} \sum_{m \neq i} |\boldsymbol{\mu}_j| |\boldsymbol{\mu}_m| \langle \boldsymbol{\chi}_{ij}^r \cdot \boldsymbol{\chi}_{im}^r \rangle \\ &= \mu_i^2 \sum_{j=1}^N \mu_j^2 (\chi^r)^2\end{aligned}\quad (42)$$

Substituting the approximation

$$\left\langle \sqrt{\frac{1}{N} \sum_{i=1}^N (\Delta\mathbf{F}_i)^2} \right\rangle \approx \sqrt{\frac{1}{N} \sum_{i=1}^N \langle (\Delta\mathbf{F}_i)^2 \rangle}$$

into (38) and using the term derived in (42) we can get an expression for the configurational average value $\langle\Delta F\rangle$.

$$\begin{aligned}\langle\Delta F\rangle &\approx \sqrt{\frac{1}{N} \sum_{i=1}^N \mu_i^2 \sum_{j=1}^N \mu_j^2 (\chi^r)^2} \\ \Rightarrow \Delta F &\approx \frac{1}{\sqrt{N}} \sum_{j=1}^N \mu_j^2 \chi^r\end{aligned}\quad (43)$$

From the definition of $\boldsymbol{\chi}_{ij}^r$ we can approximate $(\chi^r)^2$. Let $\hat{\boldsymbol{\mu}}$ and $\hat{\boldsymbol{\mu}}'$ be two unit orientation vectors of arbitrary dipoles. Then choosing the z axis of the spherical coordinate system (r, θ, ϕ) to be along $\hat{\boldsymbol{\mu}}$ means that $\omega(\hat{\boldsymbol{\mu}}, \hat{\mathbf{r}}) = \theta$. Furthermore,

$$\cos\omega(\hat{\boldsymbol{\mu}}', \hat{\mathbf{r}}) = \cos\theta \cos\omega(\hat{\boldsymbol{\mu}}, \hat{\boldsymbol{\mu}}') + \sin\theta \sin\omega(\hat{\boldsymbol{\mu}}, \hat{\boldsymbol{\mu}}') \cos\phi.$$

Using all of this information in conjunction with (40) gives

$$\begin{aligned}(\chi^r)^2 &\approx \frac{1}{L^3} \int_{r_c}^{\infty} r^2 dr \int_0^{\pi} \sin\theta d\theta \int_0^{2\pi} d\phi \left\{ [\hat{\mathbf{r}} \cos\omega(\hat{\boldsymbol{\mu}}, \hat{\boldsymbol{\mu}}') + \hat{\boldsymbol{\mu}}(\cos\theta \cos\omega(\hat{\boldsymbol{\mu}}, \hat{\boldsymbol{\mu}}') \right. \\ &\quad \left. + \sin\theta \sin\omega(\hat{\boldsymbol{\mu}}, \hat{\boldsymbol{\mu}}') \cos\phi) + \hat{\boldsymbol{\mu}}' \cos\theta] r C(r) - \hat{\mathbf{r}} \cos\theta (\cos\theta \cos\omega(\hat{\boldsymbol{\mu}}, \hat{\boldsymbol{\mu}}') \right. \\ &\quad \left. + \sin\theta \sin\omega(\hat{\boldsymbol{\mu}}, \hat{\boldsymbol{\mu}}') \cos\phi) r^3 D(r) \right\}^2.\end{aligned}$$

Based on our assumption that the positions and orientations of different particles are uncorrelated we have the following results^[5]:

$$\langle \sin^2 \theta \rangle = \langle \cos^2 \theta \rangle = \frac{1}{2}, \quad \langle \sin \theta \cos \theta \rangle = 0. \quad (44)$$

These results can be substituted into our expression for $(\chi^r)^2$ reducing the equation to a more manageable format. Wang and Holm^[33] then make further simplifications by applying the asymptotic expansion formula. This leads to the following approximation to $(\chi^r)^2$:

$$(\chi^r)^2 \approx \frac{\frac{13}{6}C_c^2 + \frac{2}{15}D_c^2 - \frac{13}{15}C_cD_c}{L^3r_c^9\alpha^4} e^{-2\alpha^2r_c^2} \quad (45)$$

where

$$C_c = 4\alpha^4r_c^4 + 6\alpha^2r_c^2 + 3, \\ D_c = 8\alpha^6r_c^6 + 20\alpha^4r_c^4 + 30\alpha^2r_c^2 + 15.$$

Taking the square root of (45) and substituting the result into (43) gives

$$\Delta F^r \approx \sum_{j=1}^N \mu_j^2 e^{-\alpha^2r_c^2} \sqrt{\frac{\frac{13}{6}C_c^2 + \frac{2}{15}D_c^2 - \frac{13}{15}C_cD_c}{L^3r_c^9\alpha^4 N}} \quad (46)$$

The real space cut-off error in the torque is derived by following the same method used for the force cut-off error, which results in (47).

$$\Delta \tau^r \approx \sum_{j=1}^N \mu_j^2 e^{-\alpha^2r_c^2} \sqrt{\frac{\frac{1}{2}B_c^2 + \frac{1}{5}C_c^2}{L^3r_c^7\alpha^4 N}} \quad (47)$$

with

$$B_c = 2\alpha^2r_c^2 + 1$$

and C_c as stated before.

Whilst the derivation for the real space cut-off error for the total potential energy is also calculated in the same way as the force there is a small difference. Since the interaction energy between two dipoles is split equally between them the sum of the mean square contains each pair's contribution twice in this case. Thus, the error is taken to be half of this sum.

$$\Delta U^r \approx \sum_{j=1}^N \mu_j^2 e^{-\alpha^2r_c^2} \sqrt{\frac{\frac{1}{4}B_c^2 + \frac{1}{15}C_c^2 - \frac{1}{6}B_cC_c}{L^3r_c^7\alpha^4 N}} \quad (48)$$

The cut-off errors given in (46), (47) and (48) all contain the exponential $e^{-\alpha^2r_c^2}$. So, to keep the errors small we require $\alpha r_c > 1$ and hence the error estimates can be simplified by only keeping the highest powers of αr_c . Wang and Holm^[33] did this for an error of

$e^{-\pi^2} \approx 5 \times 10^{-5}$ to get the following simplified versions:

$$\begin{aligned}\Delta F^r &\approx 8\alpha^4 \sum_{j=1}^N \mu_j^2 e^{-\alpha^2 r_c^2} \sqrt{\frac{2r_c^3}{15NL^3}}, \\ \Delta \tau^r &\approx 4\alpha^2 \sum_{j=1}^N \mu_j^2 e^{-\alpha^2 r_c^2} \sqrt{\frac{r_c}{5NL^3}}, \\ \Delta U^r &\approx 4\alpha^2 \sum_{j=1}^N \mu_j^2 e^{-\alpha^2 r_c^2} \sqrt{\frac{r_c}{15NL^3}}.\end{aligned}$$

An advantage of this format is that it makes it easier to determine how the error depends on the parameters r_c and α , which is useful when deciding how to optimise them as discussed in §3.3.3.

3.3.2 Errors in Reciprocal Space

Further to the assumptions made in §3.3.1 we now assume that the radial distribution function of the particles, which represents the variation in density as a function of the distance from a certain particle, approximates to unity at all distances.

From the reciprocal space force term (34) we can see that the reciprocal space cut-off in the error of the force acting on particle i is given by

$$\Delta \mathbf{F}_i^k = \sum_{j=1}^N \sum_{\substack{\mathbf{k} \\ k > k_c}} \frac{4\pi \mathbf{k}}{L^3 k^2} (\boldsymbol{\mu}_i \cdot \mathbf{k})(\boldsymbol{\mu}_j \cdot \mathbf{k}) e^{-\left(\frac{\pi k}{\alpha L}\right)^2} \sin(\mathbf{k} \cdot \mathbf{r}_{ij}). \quad (49)$$

In (49) the diagonal term (when $j = i$) in the sum is not reliant on the positioning of the particles and so provides a systematic contribution to the reciprocal cut-off error. In the force and torque cut-off errors this term is zero and so the systematic contribution is not present. It will, however, become important in the derivation of the cut-off error in the total potential.

The off-diagonal terms in (49) do depend on position and will have alternating signs as a result of the nature of the sin function. We can deal with these using the same statistical methods used in the approximation of the cut-off error in real space. Defining the reciprocal space cut-off error in the same format as (39) we get

$$\Delta \mathbf{F}_{i,off}^k = |\boldsymbol{\mu}_i| \sum_{\substack{j=1 \\ j \neq i}}^N |\boldsymbol{\mu}_j| \boldsymbol{\chi}_{ij}^k \quad (50)$$

with

$$\boldsymbol{\chi}_{ij}^k = \sum_{\substack{\mathbf{k} \\ k > k_c}} \frac{4\pi \mathbf{k}}{L^3} \cos \omega(\hat{\boldsymbol{\mu}}_i, \hat{\mathbf{k}}) \cos \omega(\hat{\boldsymbol{\mu}}_j, \hat{\mathbf{k}}) e^{-\left(\frac{\pi k}{\alpha L}\right)^2} i e^{-i\mathbf{k} \cdot \mathbf{r}_{ij}}$$

where $\hat{\mathbf{k}}$ is a unit vector along \mathbf{k} and the sin term has been rewritten using the identity given in (4) and the symmetrical nature of the summation over \mathbf{k} . Once more assuming that the positions and orientations are random gives us the following result

$$\begin{aligned}\langle(\Delta\mathbf{F}_i^k)^2\rangle &= \mu_i^2 \sum_{j \neq i} \sum_{m \neq i} |\boldsymbol{\mu}_j| |\boldsymbol{\mu}_m| \langle \boldsymbol{\chi}_{ij}^k \cdot \boldsymbol{\chi}_{im}^k \rangle \\ &= \mu_i^2 \sum_{j=1}^N \mu_j^2 (\chi^k)^2\end{aligned}$$

where again χ^k does not depend on i or j and δ_{jm} is the Kronecker delta function.

As before we use the definition of $\boldsymbol{\chi}_{ij}^k$ to write

$$\begin{aligned}(\chi^k)^2 &\approx \left(\frac{4\pi}{L^3}\right)^2 \int_{k_c}^{\infty} e^{-2(\frac{\pi k}{\alpha L})^2} k^4 dk \int_0^{\pi} \sin \theta d\theta \\ &\quad \times \int_0^{2\pi} \cos^2 \theta [\cos \theta \cos \omega(\hat{\boldsymbol{\mu}}, \hat{\boldsymbol{\mu}}') + \sin \theta \sin \omega(\hat{\boldsymbol{\mu}}, \hat{\boldsymbol{\mu}}') \cos \phi]^2 d\phi.\end{aligned}\quad (51)$$

Applying the same process as in the derivation of the real space cut-off error Wang and Holm^[33] simplify (51) to give

$$(\chi^k)^2 \approx \frac{128\pi^2 \alpha^2 k_c^3}{15L^5} e^{-2(\frac{\pi k_c}{\alpha L})^2}.$$

Hence, the reciprocal space cut-off error in the forces is

$$\Delta F^k \approx \frac{4\alpha}{L^2} \sum_{j=1}^N \mu_j^2 e^{-(\frac{\pi k_c}{\alpha L})^2} \sqrt{\frac{2\pi k_c^3}{15N}}.\quad (52)$$

where we have not distinguished between diagonal and off diagonal contributions since the diagonal contribution is zero in this case.

Calculating the reciprocal space cut-off error for torque in the same way as for force and ignoring the zero diagonal contribution gives

$$\Delta \tau^k \approx \frac{4\alpha}{L^2} \sum_{j=1}^N \mu_j^2 e^{-(\frac{\pi k_c}{\alpha L})^2} \sqrt{\frac{\pi k_c}{5N}}.$$

Following this method again the reciprocal space error in the total interaction potential is calculated, taking into account the systematic contribution from the diagonal term. As was the situation in the real space case the sum of the mean square of the total interaction energy double counts each pair of interactions and this has been taken into account to get the following results:

$$\Delta U^k = \Delta U_{off}^k + \Delta U_{diag}^k$$

where

$$\begin{aligned}
\Delta U_{off}^k &\approx \frac{4\alpha}{L^2} \sum_{j=1}^N \mu_j^2 e^{-(\frac{\pi k_c}{\alpha L})^2} \sqrt{\frac{\pi k_c}{15N}} \\
\Delta U_{diag}^k &= \frac{1}{2\sqrt{N}} \sum_{i=1}^N \sum_{\substack{\mathbf{k} \\ k > k_c}} \frac{4\pi}{L^3} \mu_i^2 e^{-(\frac{\pi k_c}{\alpha L})^2} \cos^2 \omega(\hat{\boldsymbol{\mu}}_i, \hat{\mathbf{k}}) \\
&\approx \frac{2\pi}{L^3 \sqrt{N}} \sum_{j=1}^N \mu_j^2 \int_{k_c}^{\infty} e^{-(\frac{\pi k_c}{\alpha L})^2} k^2 dk \int_0^{\pi} \sin \theta d\theta \int_0^{2\pi} \cos^2 \theta d\phi \\
&\approx \frac{4\alpha^2 k_c}{3L \sqrt{N}} \sum_{j=1}^N \mu_j^2 e^{-(\frac{\pi k_c}{\alpha L})^2}.
\end{aligned}$$

Comparing the diagonal and off diagonal terms we can see that the systematic contribution to the reciprocal space error is a factor of $\sim L\alpha\sqrt{k_c}$ larger than the off-diagonal term. Since this is much greater than one this term dominates the reciprocal space error in the total interaction energy.

3.3.3 Optimising the Parameters

Wang and Holm^[33] give the overall computing time required for using the Ewald summation to calculate the forces as

$$T = a_r N^2 \left(\frac{r_c}{L}\right)^3 + a_k N k_c^3$$

where a_r and a_k can only be determined through numerical work and depend on how the code is implemented. The numerical work carried out by Wang and Holm^[33] (in which they used standard Fourier transforms rather than FFTs) found them to be $a_r = 2.5\mu s$ and $a_k = 0.7\mu s$ for their implementation and so we shall proceed using these values. Using (46) and (52) we have the following constraints on the error bounds

$$\frac{\delta}{\sqrt{2}} = \sum_{j=1}^N \mu_j^2 e^{-\alpha^2 r_c^2} \sqrt{\frac{\frac{13}{6} C_c^2 + \frac{2}{15} D_c^2 - \frac{13}{15} C_c D_c}{L^3 r_c^9 \alpha^4 N}} \quad (53)$$

$$\frac{\delta}{\sqrt{2}} = \frac{4\alpha}{L^2} \sum_{j=1}^N \mu_j^2 e^{-(\frac{\pi k_c}{\alpha L})^2} \sqrt{\frac{2\pi k_c^3}{15N}} \quad (54)$$

where δ is the required accuracy. If $\delta \leq 5 \times 10^{-5}$ then the simplified version of the real space cut-off error given by Wang and Holm^[33] could be used instead of (46). From (53) and (54) we get the following relationships between α and the two cut-offs:

$$r_c(\alpha) \approx -A \frac{\sqrt{\ln \delta}}{\alpha}, \quad k_c(\alpha) \approx -B \alpha \sqrt{\ln \delta}.$$

Substituting these into the equation for overall computation time alongside the values for a_r and a_k and differentiating with respect to α gives:

$$T \approx -2.5N^2 \left(\frac{\sqrt{\ln \delta}}{L\alpha} \right)^3 - 0.7N(B\alpha\sqrt{\ln \delta})^3$$

$$\Rightarrow \frac{\delta T}{\delta \alpha} \approx 7.5N^2 \left(\frac{(\sqrt{\ln \delta})^3}{L^3\alpha^4} \right) - 2.1N(B\sqrt{\ln \delta})^3\alpha^2.$$

Setting this equal to zero in order to find the minimum value of α we see that $\alpha \propto N^{\frac{1}{6}}$, which means that $k_c \propto N^{\frac{1}{6}}$ as well and $r_c \propto N^{-\frac{1}{6}}$. If the parameters are chosen in this way the overall computation time becomes proportional to $N^{\frac{3}{2}}$ where the required accuracy decides the proportionality constant^[33].

4 Simulation

The code controlling the simulation run in this section is all written in the C programming language and was provided by Dr. Zuowei Wang of the University of Reading (supervisor for this project). As a result its implementation is not discussed here.

The details of finely controlled simulations run from this code have been published previously^[19,33]. However, for this project further simulations were run to provide a cursory visualisation of the behaviours of ferrofluids discussed in §1 and demonstrate some of the ideas discussed in this report. This required a basic knowledge of the code involved, particularly how to adjust the various parameters in the program to achieve the desired result. Visual Molecular Dynamics (VMD) software was also utilised to produce the diagrams that are included in this section^[18]. Finally, since the output from the original code was not in the required format two trivial programs in C++ were created to convert output from the simulation into one format that could be graphed and one that was compatible with the VMD software. The diagrams in this section only show one simulation box; remember that we are dealing with a system of adjoining boxes displaying identical behaviour.

To allow for comparison two ferrofluids with different particle sizes were simulated. The small particles have a diameter of 10nm and the larger ones have a 16nm diameter. In each case the simulation was run with 1000 particles, which were to account for 5% of the volume of the simulation box, since at this density it is easier to see what is happening pictorially. In order to satisfy all of the conditions that have just been specified the program used the following relationship to calculate the size of the simulation box required:

$$V = \frac{N \pi \sigma^3}{\phi 6}$$

where ϕ is the volume fraction, σ is the particle size and V is the volume of the simulation box^[35]. Substituting the relevant values in and then taking the cubic root (since we are dealing with a cubic simulation box) gives $L = 21.9$ for the small particles and $L = 35$ for the large particles.

The root mean square (rms) error, as defined in §3.3, was set to be $\Delta F \leq 10^{-4}$ and the corresponding optimal values of α , r_c and k_c were selected in the way discussed in §3.3.3. The time step used was $\Delta t = 2.5 \times 10^{-3}$, which is sufficiently small to keep the leapfrog scheme (§2.1.1) stable.

4.1 Average Cluster Size

Figure 7 looks at the average size of clusters in our system as time progresses. As might be expected a cluster is a group of particles that are touching and the size is simply how many particles are in that cluster. In order to calculate cluster size the program is set up

to consider dipoles as part of the same cluster when the dipolar interaction energy is less than a value predetermined by

$$U_{bond} = -1.4\lambda k_B T$$

where λ is the dipolar coupling constant ($= 4$ in this case) and $k_B T$ is the temperature measured in Kelvin ($= 1$ in this case)^[19,35]. This is equivalent to 70% of the dipolar interaction energy between two touching particles with their dipole moments perfectly aligned. The average cluster size is then taken to be

$$\langle S \rangle = \frac{\sum_s s n_s}{\sum_s n_s}$$

where n_s is the number of clusters that have size s ^[19,35].

Cluster size is something that cannot be measured in experimental work and so this highlights the importance of simulations in enabling scientists to see more than they can in a lab. Kantorovich et al.^[21] go into detail about the struggle of experimental work to even obtain proof of the chain formations recognised so easily in simulative works. Many other researchers have published articles in recent years regarding the aggregation (formation of clusters) of magnetic fluids, so data such as that taken from this simulation are an invaluable contribution to the field^[8,9,30].

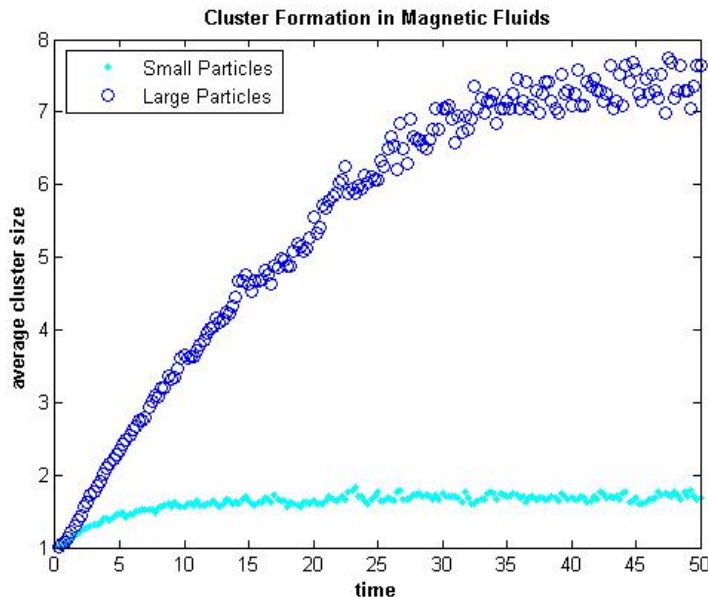


Figure 7: Comparison of average cluster size over time for large and small particles after the application of external magnetic field.

Since we are starting from a random configuration of the particles we would expect the average cluster size to take value 1 at time $t = 0$. This is clearly evident in Figure 7. Figures 8 and 10 show the starting configurations for the small particles and the large

particles respectively, and we can see that the set-up indeed appears to be random. In Figures 9 and 11 we can see the position of the particles at the end of the simulation. Although the chain formation is evident in both sets of particles there is clearly more structure in the system of larger particles. The graph verifies this as we can see that the large particles form clusters four times the size of the small particles in the equivalent time frame. This demonstrates how essential the definition of touching stated earlier is since in Figure 9 the clusters appear to be much larger for small particles than the data indicates. Also, from Figure 7 we can see how soon after the external field is applied aggregation begins.

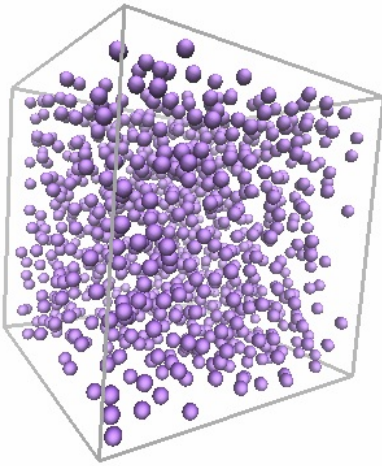


Figure 8: Starting configuration of small particles under external magnetic field.

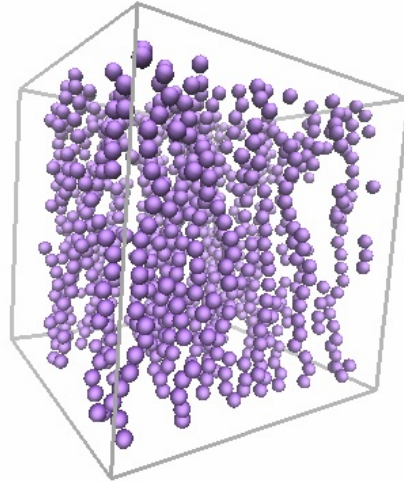


Figure 9: Final configuration of small particles under external magnetic field.

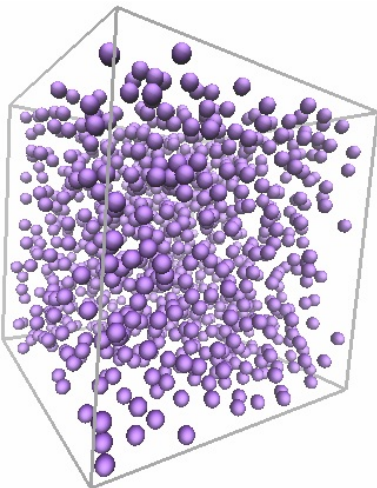


Figure 10: Starting configuration of large particles under external magnetic field.

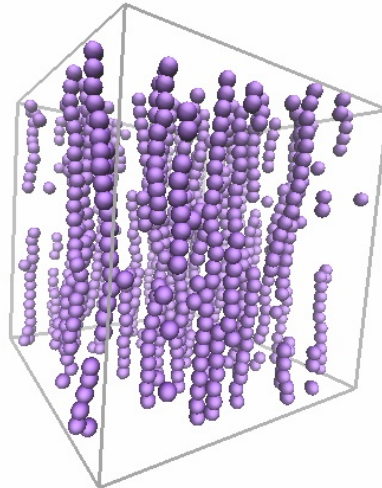


Figure 11: Final configuration of large particles under external magnetic field.

It may appear in Figure 7 that there are several measurements taken at some time steps. This is not the case; it is simply a result of the scale of the graph in comparison to the size of the time step.

There are other results that can be studied using simulations, such as magnetisation response (how quickly the particles react to the presence of the magnetic field). Results from simulations where the conditions are changed by varying any of the inherent parameters are also easily achieved. However, these ideas are not discussed in great detail here as there is limited time to complete this work and running many simulations can be quite time consuming. The aim of this section was merely to provide a visual context to the behaviours of magnetic fluids and to demonstrate the clarity of simulation data in contrast with experimental work in some instances.

5 Dealing with a Confined Geometry

The Ewald method discussed in §3 is designed for application to a standard three dimensional geometry. In this section the method is adapted to enable its use in a geometry that is confined in one direction (called a slab geometry). The method used previously is no longer valid in this situation since periodicity in the confined direction is lost and the formulae were derived assuming periodicity in all three directions.

Slab geometries are found in many scenarios of interest to physicists and chemists including fluids contained between two walls, electrolyte solutions between charged surfaces and transport through membranes^[2,6]. More interestingly in relation to this project, slab geometries are also characteristic of thin films of ferrofluids, such as those simulated in §4.

5.1 What is a Confined Geometry?

In order to create a confined, or slab, geometry we start with the standard three dimensional periodic system discussed in §2.2 and insert two planes parallel to the top and bottom of the simulation cube. The substance being modelled (magnetic fluids in our case) is then contained between these walls, as demonstrated very crudely in Figure 12. So, when we model our system the strips containing the fluid are now infinitely periodic in only two directions and are finite in the third. This leads to the creation of what is termed a $2D+H$ system; i.e. two dimensions are as before but the third is restricted according to the height, H , of the strips containing fluid.

Throughout this section the word ‘strip’ is used to represent the cuboids that the simulation fluid is contained in and ‘gap’ refers to the spaces in between the strips that are empty. The term ‘standard geometry’ refers to the three dimensional periodic system we looked at in §3 whilst both ‘slab geometry’ and ‘confined geometry’ describe the new $2D+H$ setup.

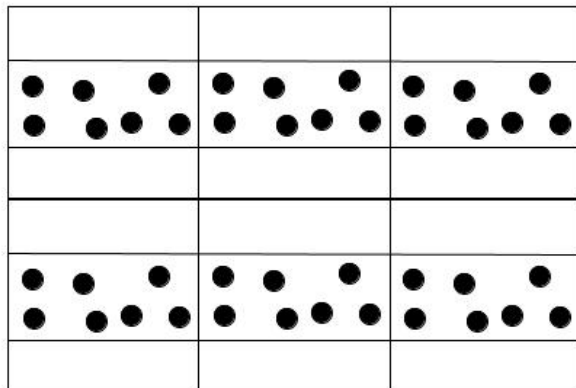


Figure 12: Simplified two-dimensional representation of confined geometry set up.

One way to approach this scenario would be to ensure that the gaps between strips are sufficiently large to eliminate interaction between particles in different strips. However, this is computationally expensive due to the large dimensions required to cancel out such long range interactions. So, instead we introduce a correction term, as detailed in §5.2, in order to maintain equilibrium and keep computational efforts within acceptable limits.

5.2 Ewald Method for a Confined Geometry

Arnold et al.^[2] first proposed the EW3DLC (3 dimensional Ewald summation with layer correction) approach for dealing with a slab geometry and derived this for charge-charge interactions. Essentially the method operates by firstly amending the summation order of the Ewald summation to sum slab-wise and secondly corrects for the introduction of interactions between strips. Bródka^[4] later responded with an alternate version of the electrostatic layer correction (ELC term), which was also adapted to model dipole-dipole interactions^[5]. The derivations in this section are based heavily on Bródka’s work.

Although i has been used as the primary summation index in the previous sections of this report it becomes problematic when working in a confined geometry due to the introduction of imaginary numbers in some of the calculations. Hence, in this section the summation index k will be used instead. This is not to be confused with the superscript k that represents Fourier space terms.

As with the derivation of the original Ewald method it is easiest to apply the theory to the situation of charge-charge interactions (§5.2.1) to begin with and then extend it to account for dipole-dipole interactions (§5.2.2) by replacing q_k with $\boldsymbol{\mu}_k \cdot \nabla_{\mathbf{r}_k}$ as before. In the following derivations we are assuming we have the dielectric constant $\epsilon_s = 1$ as in previous calculations, so this is not stated explicitly in the formulae.

5.2.1 Charge-Charge Interactions

To begin with we take a simulation box with dimensions $L_x \times L_y \times L_z$ but we confine the particles to a cuboid of dimensions $L_x \times L_y \times H$ (where $L_z > H$) contained within the simulation box, which corresponds to adding in the walls. This set up is then repeated periodically as demonstrated in Figure 12. Note that no further restrictions have been placed on H other than that it must be less than L . As before, we make the assumption that the total system is charge neutral and furthermore, that each strip is also charge neutral.

In §3.1 the simulation boxes were summed in a spherical manner (see Figure 4), which means that the number of image simulation boxes considered grows faster than the number of boxes considered in the primary layer of boxes. In a confined geometry this results in large errors as we are effectively including more unwanted terms as opposed to the ones we desire. Yeh and Berkowitz^[36] solve this problem by adding the following term to the

potential (see also Arnold et al.^[2]):

$$U_c^{slabsum} = \frac{2\pi M_z^2}{V} \quad (55)$$

where $V = L_x L_y L_z$ is the volume of a simulation box and $M = \sum_{k=1}^N q_k \mathbf{r}_k$ with M_z being the z component of this. This results in the summation being performed slab-wise rather than the spherical manner considered before, which is far more useful. Slab-wise summation means that we first consider the original strip by adding images of the original simulation box in the x and y axes directions and then add simulation boxes in symmetrical pairs (above and below) in the z axis direction. This new term already takes into account the change of behaviour at the surface of the system and so the surface term used in §3.1 is no longer required. On inspection the similarities between this term and the surface term used previously are obvious.

The real space part of the Ewald summation is almost identical in a slab geometry to the standard three dimensional set-up. It is given by

$$U_c^{slabr} = \frac{1}{2} \sum_{\mathbf{n} \in \mathbb{Z}^2} \left(\sum_{k=1}^N \sum_{j=1}^N q_k q_j \frac{\text{erfc}(\alpha |\boldsymbol{\gamma}_{kj} + \mathbf{n}, z_{kj}|)}{|\boldsymbol{\gamma}_{kj} + \mathbf{n}, z_{kj}|} \right)$$

where $\boldsymbol{\gamma}_{kj}$ describes the projection of \mathbf{r}_{kj} onto the (x, y) plane and $\mathbf{n} = (n_x L_x, n_y L_y)$. In fact by clever choice of α we can restrict the real space summation to our basic simulation box and then for this term we can use (9)^[7]. We will assume that α has been chosen in such a way as to enable us to use the real space term derived previously. The self-interaction term is the same in both geometries and so we can use (17) in the slab geometry potential too.

The Fourier space summation in a slab geometry is given by

$$U_c^{slabk} = \frac{\pi}{2L_x L_y} \sum_{\mathbf{G} \neq \mathbf{0}} \sum_{k=1}^N \sum_{j=1}^N q_k q_j e^{i\mathbf{G} \cdot \boldsymbol{\gamma}_{kj}} \frac{1}{G} \left[e^{Gz} \text{erfc} \left(\frac{G}{2\alpha} + \alpha z \right) + e^{-Gz} \text{erfc} \left(\frac{G}{2\alpha} - \alpha z \right) \right] \quad (56)$$

where $\mathbf{G} = 2\pi \left(\frac{k_x}{L_x}, \frac{k_y}{L_y}, \frac{k_z}{L_z} \right)$ is a vector in reciprocal space and $G = |\mathbf{G}|$ ^[7]. This term can be rearranged using results taken from the derivation of the two dimensional Ewald summation and then after analytical solving of the integral introduced (56) becomes

$$U_c^{slabk} = \frac{2\pi}{V} \sum_{\mathbf{G} \neq \mathbf{0}} \sum_{k=1}^N \sum_{j=1}^N q_k q_j \frac{1}{G^2} e^{-\frac{G^2}{4\alpha^2}} \cos(\mathbf{G} \cdot \mathbf{r}_{kj}). \quad (57)$$

Bródka and Grzybowski^[7] provide interim steps in the transition from (56) to (57). They also demonstrate how the Fourier space term when $\mathbf{G} = \mathbf{0}$ reduces to (55), the term that compensates for the change in summation technique. At a glance we can see that the

expression in (57) is basically the same as the Fourier term in our previous derivation with \mathbf{k} and k replaced by \mathbf{G} and G respectively. From the definition of \mathbf{G} we can see that this makes sense.

Now that we have amended our Ewald summation from §3 to fit our new geometry we need to subtract the inter-strip interactions from our total potential. Bródka^[4] takes the difference between the reciprocal space term for a two dimensional system and the equivalent term derived in three dimensions. Then analysis of the convergence of each term in the resulting expression is discussed in order to simplify it. This yields the following expression for the ELC term^[4-6]:

$$U_c^{ELC} = -\frac{\pi}{L_x L_y} \sum_{\mathbf{G}_\gamma \neq 0} \frac{1}{G_\gamma (e^{G_\gamma L_z} - 1)} \sum_{k=1}^N \sum_{j=1}^N [S_{c+,k}(\mathbf{G}_\gamma) S_{c-,j}^*(\mathbf{G}_\gamma) + S_{c-,k}(\mathbf{G}_\gamma) S_{c+,j}^*(\mathbf{G}_\gamma)] \quad (58)$$

where \mathbf{G}_γ describes the projection of \mathbf{G} onto the (x, y) plane and

$$S_{c\pm,k}(\mathbf{G}_\gamma) = q_k e^{i\mathbf{G}_\gamma \cdot \boldsymbol{\gamma}_k} e^{\pm G_\gamma z_k}$$

is the structure factor. The $*$ notation used on some of the terms indicates complex conjugates, which are taken to be

$$S_{c\pm,j}^*(\mathbf{G}_\gamma) = q_j e^{-i\mathbf{G}_\gamma \cdot \boldsymbol{\gamma}_j} e^{\pm G_\gamma z_j}.$$

Combining the components (9), (57), (17), (55) and (58) we get the final expression for the Ewald summation with the added ELC term for charge-charge interactions.⁶

$$\begin{aligned} U_c^{slab} &= U_c^r + U_c^{slabk} + U_c^{self} + U_c^{slabsum} + U_c^{ELC} \\ &= \sum_{k=1}^N \sum_{j=1}^N q_k q_j \left[\frac{1}{2} \sum_{\mathbf{n} \in \mathbb{Z}^3} \left(\frac{\text{erfc}(\alpha |\mathbf{r}_{kj} + \mathbf{n}|)}{|\mathbf{r}_{kj} + \mathbf{n}|} \right) + \frac{2\pi}{V} \sum_{\mathbf{G} \neq 0} \frac{1}{G^2} e^{-\frac{G^2}{4\alpha^2}} \cos(\mathbf{G} \cdot \mathbf{r}_{kj}) \right. \\ &\quad \left. - \frac{\pi}{L_x L_y} \sum_{\mathbf{G}_\gamma \neq 0} \frac{1}{G_\gamma (e^{G_\gamma L_z} - 1)} [S_{c+,k}(\mathbf{G}_\gamma) S_{c-,j}^*(\mathbf{G}_\gamma) + S_{c-,k}(\mathbf{G}_\gamma) S_{c+,j}^*(\mathbf{G}_\gamma)] \right] \\ &\quad - \frac{\alpha}{\sqrt{\pi}} \sum_{k=1}^N q_k^2 + \frac{2\pi M_z^2}{V} \end{aligned}$$

5.2.2 Dipole-Dipole Interactions

Using the substitution $\boldsymbol{\mu}_k \cdot \nabla_{\mathbf{r}_k}$ in place of q_k in the derivations for charge-charge interactions clearly leads us directly to the real space and self terms, (21) and (23), that we had in the standard Ewald summation. We can also directly achieve the reciprocal space

⁶Remember that we have chosen α in such a way that the real space summation is contained within the simulation box.

term for dipole-dipole interactions^[5,7,15].

$$U_d^{slabk} = \frac{2\pi}{V} \sum_{\mathbf{G} \neq 0} \sum_{k=1}^N \sum_{j=1}^N (\boldsymbol{\mu}_k \cdot \mathbf{G})(\boldsymbol{\mu}_j \cdot \mathbf{G}) \frac{1}{G^2} e^{-\frac{G^2}{4\alpha^2}} \cos(\mathbf{G} \cdot \mathbf{r}_{kj}) \quad (59)$$

The term correcting for the change in summation technique takes the same form as (55) but the definition of M has changed. So, we have

$$U_d^{slabsum} = \frac{2\pi M_z^2}{V} \quad (60)$$

where $M^2 = \sum_{k=1}^N \sum_{j=1}^N \boldsymbol{\mu}_k \cdot \boldsymbol{\mu}_j$ and M_z^2 is again the z component of this.

In the new ELC term for dipolar interactions the only change is to the format of the functions $S_{\pm,k}(\mathbf{G}_\gamma)$ and $S_{\pm,j}^*(\mathbf{G}_\gamma)$.

$$U_d^{ELC} = -\frac{\pi}{L_x L_y} \sum_{\mathbf{G}_\gamma \neq 0} \frac{1}{G_\gamma (e^{G_\gamma L_z} - 1)} \sum_{k=1}^N \sum_{j=1}^N [S_{d+,k}(\mathbf{G}_\gamma) S_{d-,j}^*(\mathbf{G}_\gamma) + S_{d-,k}(\mathbf{G}_\gamma) S_{d+,j}^*(\mathbf{G}_\gamma)] \quad (61)$$

where

$$S_{d\pm,k}(\mathbf{G}_\gamma) = (i\boldsymbol{\mu}_k^\gamma \cdot \mathbf{G}_\gamma \pm \mu_k^z \cdot G_\gamma) e^{i\mathbf{G}_\gamma \cdot \boldsymbol{\gamma}_k} e^{\pm G_\gamma z_k},$$

and

$$S_{d\pm,j}^*(\mathbf{G}_\gamma) = (-i\boldsymbol{\mu}_j^\gamma \cdot \mathbf{G}_\gamma \pm \mu_j^z \cdot G_\gamma) e^{-i\mathbf{G}_\gamma \cdot \boldsymbol{\gamma}_j} e^{\pm G_\gamma z_j}.$$

In the above result $\boldsymbol{\mu}_k^\gamma$ and μ_k^z denote components of the dipole moment $\boldsymbol{\mu}_k$ that are parallel and perpendicular to the (x, y) plane respectively. Combining all the terms discussed in this section ((21), (59), (23), (60) and (61)) gives the overall dipole-dipole potential in a confined geometry.⁷

$$\begin{aligned} U_d^{slab} &= U_d^r + U_d^{slabk} + U_d^{self} + U_d^{slabsum} + U_d^{ELC} \\ &= \sum_{k=1}^N \sum_{j=1}^N \left[\frac{1}{2} \sum_{\mathbf{n} \in \mathbb{Z}^3} [(\boldsymbol{\mu}_k \cdot \boldsymbol{\mu}_j) B(|\mathbf{r}_{kj} + \mathbf{n}|) - (\boldsymbol{\mu}_k \cdot (\mathbf{r}_{kj} + \mathbf{n}))(\boldsymbol{\mu}_j \cdot (\mathbf{r}_{kj} + \mathbf{n})) C(|\mathbf{r}_{kj} + \mathbf{n}|)] \right. \\ &\quad + \frac{2\pi}{V} \sum_{\mathbf{G} \neq 0} (\boldsymbol{\mu}_k \cdot \mathbf{G})(\boldsymbol{\mu}_j \cdot \mathbf{G}) \frac{1}{G^2} e^{-\frac{G^2}{4\alpha^2}} \cos(\mathbf{G} \cdot \mathbf{r}_{kj}) \\ &\quad \left. - \frac{\pi}{L_x L_y} \sum_{\mathbf{G}_\gamma \neq 0} \frac{1}{G_\gamma (e^{G_\gamma L_z} - 1)} [S_{d+,k}(\mathbf{G}_\gamma) S_{d-,j}^*(\mathbf{G}_\gamma) + S_{d-,k}(\mathbf{G}_\gamma) S_{d+,j}^*(\mathbf{G}_\gamma)] \right] \\ &\quad - \sum_{k=1}^N \frac{2\alpha^3 \mu_k^2}{3\sqrt{\pi}} + \frac{2\pi M_z^2}{V} \end{aligned}$$

⁷Again recall that we have chosen α in such a way that the real space summation is contained within the simulation box.

A direct comparison with the Ewald method derived for dipolar interactions in a three dimensionally periodic system indicates that the main change is the addition of the final term. The only other differences are the change of notation in the reciprocal space term and the requirement to deal with the z component only in the final term. An additional consideration is that α must be chosen in such a way as to keep the real space summation within the simulation box to avoid complicating this term.

5.3 Application of Ewald Method for a Confined Geometry

As we did when looking at the standard three dimensional Ewald summation we are only going to look at applications and errors in relation to dipolar interactions, so we will drop the subscript d from our notation. All of the considerations to be made when programming the three dimensional Ewald summation remain the same for a slab geometry. It is simply the terms involved that have changed. As a result the program used in §4 could be utilised to simulate the new geometry with only minor changes required. These are, chiefly, the addition of the extra term in the Ewald summation and the introduction of the walls into the program.

Clearly since we are using the same real space term as in the standard geometry the force and torque for this term will be the same as those given in §3.2. The self term is also the same as was used in the standard three dimensional geometry and hence it once again does not contribute to either the force or the torque.

The discussions in this section relating to the contribution of the new ELC and summation terms to the force and torque are only preliminary. I was unable to find any publications that have calculated them previously and due to time constraints have been unable to carry out any numerical work to examine their accuracy.

5.3.1 Force

As discussed in §3.2.1 the force, \mathbf{F}_k , acting on a particular particle, k is found by differentiating U^{slab} with respect to \mathbf{r}_k and negating the answer. We can state the force contribution in reciprocal space directly as a result of the similarities between (59) and (22):

$$\mathbf{F}_k^{slabk} = \frac{4\pi}{V} \sum_{j=1}^N \sum_{\substack{\mathbf{G} \in \mathbb{Z}^3 \\ \mathbf{G} \neq \mathbf{0}}} \frac{\mathbf{G}}{G^2} e^{-\left(\frac{\pi G}{\alpha L}\right)^2} (\boldsymbol{\mu}_k \cdot \mathbf{G})(\boldsymbol{\mu}_j \cdot \mathbf{G}) \sin(\mathbf{G} \cdot \mathbf{r}_{kj}).$$

There is no contribution to the force from the summation method term, since it is not dependent on the position of individual particles. Hence, it only remains to calculate the ELC term's contribution to the overall force. Although \mathbf{r}_k is not explicitly present in this

term it is contained within γ_k , its representation in the (x, y) plane. So we have

$$\begin{aligned}
\mathbf{F}_k^{ELC} &= -\frac{\partial(U_k^{ELC})}{\partial \mathbf{r}_k} \\
&= -\frac{\partial(U_k^{ELC})}{\partial \gamma_k} \hat{\gamma}_k - \frac{\partial(U_k^{ELC})}{\partial z_k} \hat{z}_k \\
&= \frac{2\pi}{L_x L_y} \sum_{\mathbf{G}_\gamma \neq 0} \frac{1}{G_\gamma (e^{G_\gamma L_z} - 1)} \sum_{j=1}^N \left\{ \frac{\partial}{\partial \gamma_k} [S_{+,k}(\mathbf{G}_\gamma) S_{-,j}^*(\mathbf{G}_\gamma) + S_{-,k}(\mathbf{G}_\gamma) S_{+,j}^*(\mathbf{G}_\gamma)] \hat{\gamma}_k \right. \\
&\quad \left. + \frac{\partial}{\partial z_k} [S_{+,k}(\mathbf{G}_\gamma) S_{-,j}^*(\mathbf{G}_\gamma) + S_{-,k}(\mathbf{G}_\gamma) S_{+,j}^*(\mathbf{G}_\gamma)] \hat{z}_k \right\} \quad (62)
\end{aligned}$$

where \hat{z}_k and $\hat{\gamma}_k$ are unit vectors in the relevant directions. Differentiating $S_{\pm,k}(\mathbf{G}_\gamma)$ with respect to γ_k gives

$$\frac{\partial}{\partial \gamma_k} (S_{\pm,k}(\mathbf{G}_\gamma)) = (i\boldsymbol{\mu}_k^\gamma \cdot \mathbf{G}_\gamma \pm \mu_k^z \cdot G_\gamma) (i\mathbf{G}_\gamma) e^{i\mathbf{G}_\gamma \cdot \boldsymbol{\gamma}_k} e^{\pm G_\gamma z_k}.$$

From this we get

$$\begin{aligned}
\frac{\partial}{\partial \gamma_k} S &= S_{-,j}^*(\mathbf{G}_\gamma) \frac{\partial}{\partial \gamma_k} S_{+,k}(\mathbf{G}_\gamma) + S_{+,j}^*(\mathbf{G}_\gamma) \frac{\partial}{\partial \gamma_k} S_{-,k}(\mathbf{G}_\gamma) \\
&= (-i\boldsymbol{\mu}_j^\gamma \cdot \mathbf{G}_\gamma - \mu_j^z \cdot G_\gamma) e^{-i\mathbf{G}_\gamma \cdot \boldsymbol{\gamma}_j} e^{-G_\gamma z_j} (i\boldsymbol{\mu}_k^\gamma \cdot \mathbf{G}_\gamma + \mu_k^z \cdot G_\gamma) (i\mathbf{G}_\gamma) e^{i\mathbf{G}_\gamma \cdot \boldsymbol{\gamma}_k} e^{G_\gamma z_k} \\
&\quad + (-i\boldsymbol{\mu}_j^\gamma \cdot \mathbf{G}_\gamma + \mu_j^z \cdot G_\gamma) e^{-i\mathbf{G}_\gamma \cdot \boldsymbol{\gamma}_j} e^{G_\gamma z_j} (i\boldsymbol{\mu}_k^\gamma \cdot \mathbf{G}_\gamma - \mu_k^z \cdot G_\gamma) (i\mathbf{G}_\gamma) e^{i\mathbf{G}_\gamma \cdot \boldsymbol{\gamma}_k} e^{-G_\gamma z_k} \\
&= [(-i\boldsymbol{\mu}_j^\gamma \cdot \mathbf{G}_\gamma - \mu_j^z \cdot G_\gamma) (i\boldsymbol{\mu}_k^\gamma \cdot \mathbf{G}_\gamma + \mu_k^z \cdot G_\gamma) e^{-G_\gamma z_j} e^{G_\gamma z_k} \\
&\quad + (-i\boldsymbol{\mu}_j^\gamma \cdot \mathbf{G}_\gamma + \mu_j^z \cdot G_\gamma) (i\boldsymbol{\mu}_k^\gamma \cdot \mathbf{G}_\gamma - \mu_k^z \cdot G_\gamma) e^{G_\gamma z_j} e^{-G_\gamma z_k}] (i\mathbf{G}_\gamma) e^{i\mathbf{G}_\gamma \cdot \boldsymbol{\gamma}_k} e^{-i\mathbf{G}_\gamma \cdot \boldsymbol{\gamma}_j} \\
&= [(-i\boldsymbol{\mu}_j^\gamma \cdot \mathbf{G}_\gamma - \mu_j^z \cdot G_\gamma) (i\boldsymbol{\mu}_k^\gamma \cdot \mathbf{G}_\gamma + \mu_k^z \cdot G_\gamma) e^{G_\gamma z_{kj}} \\
&\quad + (-i\boldsymbol{\mu}_j^\gamma \cdot \mathbf{G}_\gamma + \mu_j^z \cdot G_\gamma) (i\boldsymbol{\mu}_k^\gamma \cdot \mathbf{G}_\gamma - \mu_k^z \cdot G_\gamma) e^{G_\gamma z_{jk}}] (i\mathbf{G}_\gamma) e^{i\mathbf{G}_\gamma \cdot \boldsymbol{\gamma}_{kj}} \quad (63)
\end{aligned}$$

where $S = [S_{+,k}(\mathbf{G}_\gamma) S_{-,j}^*(\mathbf{G}_\gamma) + S_{-,k}(\mathbf{G}_\gamma) S_{+,j}^*(\mathbf{G}_\gamma)]$, $\boldsymbol{\gamma}_{kj} = \boldsymbol{\gamma}_k - \boldsymbol{\gamma}_j$ and $z_{kj} = z_k - z_j$. Differentiating $S_{\pm,k}(\mathbf{G}_\gamma)$ with respect to z_k we get

$$\frac{\partial}{\partial z_k} (S_{\pm,k}(\mathbf{G}_\gamma)) = \pm G_\gamma (i\boldsymbol{\mu}_k^\gamma \cdot \mathbf{G}_\gamma \pm \mu_k^z \cdot G_\gamma) e^{i\mathbf{G}_\gamma \cdot \boldsymbol{\gamma}_k} e^{\pm G_\gamma z_k},$$

which gives us

$$\begin{aligned}
\frac{\partial}{\partial z_k} S &= S_{-,j}^*(\mathbf{G}_\gamma) \frac{\partial}{\partial z_k} S_{+,k}(\mathbf{G}_\gamma) + S_{+,j}^*(\mathbf{G}_\gamma) \frac{\partial}{\partial z_k} S_{-,k}(\mathbf{G}_\gamma) \\
&= (-i\boldsymbol{\mu}_j^\gamma \cdot \mathbf{G}_\gamma - \mu_j^z \cdot G_\gamma) e^{-i\mathbf{G}_\gamma \cdot \boldsymbol{\gamma}_j} e^{-G_\gamma z_j} G_\gamma (i\boldsymbol{\mu}_k^\gamma \cdot \mathbf{G}_\gamma + \mu_k^z \cdot G_\gamma) e^{i\mathbf{G}_\gamma \cdot \boldsymbol{\gamma}_k} e^{G_\gamma z_k} \\
&\quad + (-i\boldsymbol{\mu}_j^\gamma \cdot \mathbf{G}_\gamma + \mu_j^z \cdot G_\gamma) e^{-i\mathbf{G}_\gamma \cdot \boldsymbol{\gamma}_j} e^{G_\gamma z_j} (-G_\gamma) (i\boldsymbol{\mu}_k^\gamma \cdot \mathbf{G}_\gamma - \mu_k^z \cdot G_\gamma) e^{i\mathbf{G}_\gamma \cdot \boldsymbol{\gamma}_k} e^{-G_\gamma z_k} \\
&= [(-i\boldsymbol{\mu}_j^\gamma \cdot \mathbf{G}_\gamma - \mu_j^z \cdot G_\gamma) G_\gamma (i\boldsymbol{\mu}_k^\gamma \cdot \mathbf{G}_\gamma + \mu_k^z \cdot G_\gamma) e^{G_\gamma z_{kj}} \\
&\quad + (-i\boldsymbol{\mu}_j^\gamma \cdot \mathbf{G}_\gamma + \mu_j^z \cdot G_\gamma) (-G_\gamma) (i\boldsymbol{\mu}_k^\gamma \cdot \mathbf{G}_\gamma - \mu_k^z \cdot G_\gamma) e^{G_\gamma z_{jk}}] e^{i\mathbf{G}_\gamma \cdot \boldsymbol{\gamma}_{kj}} \quad (64)
\end{aligned}$$

where S , γ_{kj} and z_{kj} are as defined previously. Substituting (63) and (64) into (62) gives

$$\begin{aligned} \mathbf{F}_k^{ELC} = & \frac{2\pi}{L_x L_y} \sum_{\mathbf{G}_\gamma \neq 0} \frac{1}{G_\gamma (e^{G_\gamma L_z} - 1)} \sum_{j=1}^N \left\{ [(-i\boldsymbol{\mu}_j^\gamma \cdot \mathbf{G}_\gamma - \mu_j^z \cdot G_\gamma)(i\boldsymbol{\mu}_k^\gamma \cdot \mathbf{G}_\gamma + \mu_k^z \cdot G_\gamma) e^{G_\gamma z_{kj}} \right. \\ & + (-i\boldsymbol{\mu}_j^\gamma \cdot \mathbf{G}_\gamma + \mu_j^z \cdot G_\gamma)(i\boldsymbol{\mu}_k^\gamma \cdot \mathbf{G}_\gamma - \mu_k^z \cdot G_\gamma) e^{G_\gamma z_{jk}}] (i\mathbf{G}_\gamma) e^{i\mathbf{G}_\gamma \cdot \boldsymbol{\gamma}_{kj}} \hat{\boldsymbol{\gamma}}_k \\ & + [(-i\boldsymbol{\mu}_j^\gamma \cdot \mathbf{G}_\gamma - \mu_j^z \cdot G_\gamma) G_\gamma (i\boldsymbol{\mu}_k^\gamma \cdot \mathbf{G}_\gamma + \mu_k^z \cdot G_\gamma) e^{G_\gamma z_{kj}} \\ & \left. + (-i\boldsymbol{\mu}_j^\gamma \cdot \mathbf{G}_\gamma + \mu_j^z \cdot G_\gamma) (-G_\gamma) (i\boldsymbol{\mu}_k^\gamma \cdot \mathbf{G}_\gamma - \mu_k^z \cdot G_\gamma) e^{G_\gamma z_{jk}}] e^{i\mathbf{G}_\gamma \cdot \boldsymbol{\gamma}_{kj}} \hat{\boldsymbol{z}}_k \right\}. \end{aligned}$$

As in §3.2.1 the total force is calculated by summing the contribution from each term as follows:

$$\mathbf{F}_k^{slab} = \mathbf{F}_k^r + \mathbf{F}_k^{slabk} + \mathbf{F}_k^{ELC}.$$

5.3.2 Torque

As discussed in §3.2.2 the torque, $\boldsymbol{\tau}_k$, of a particular particle, k , is calculated by employing its relationship with the electrostatic field, \mathbf{E}_k of the same particle. This involves differentiating the total potential with respect to dipole $\boldsymbol{\mu}_k$, taking the cross product with $\boldsymbol{\mu}_k$ and then negating the result.

As with the force we can write the reciprocal space torque for a slab geometry directly:

$$\boldsymbol{\tau}_k^{slabk} = -\frac{4\pi}{V} \sum_{\substack{\mathbf{G} \in \mathbb{Z}^3 \\ \mathbf{G} \neq 0}} \sum_{j=1}^N \frac{1}{G^2} (\boldsymbol{\mu}_k \times \mathbf{G}) (\boldsymbol{\mu}_j \cdot \mathbf{G}) e^{\left(\frac{-\pi G}{\alpha L}\right)^2} \cos(\mathbf{G} \cdot \mathbf{r}_{kj}).$$

The term added to alter the summation method will also contribute to the torque since there is $\boldsymbol{\mu}_k$ dependence in the definition of M . The contribution is as follows:

$$\begin{aligned} \mathbf{E}_k^{slabsum} &= -\frac{\partial(U_k^{slabsum})}{\partial \boldsymbol{\mu}_k} \\ &= -\frac{\partial(U_k^{slabsum})}{(\partial \boldsymbol{\mu}_k)_z} \hat{\boldsymbol{z}} \\ &= -\frac{4\pi}{V} \sum_{j=1}^N \frac{\partial}{\partial \boldsymbol{\mu}_k} [(\boldsymbol{\mu}_k)_z \cdot (\boldsymbol{\mu}_j)_z] \hat{\boldsymbol{z}} \\ &= -\frac{4\pi}{V} \sum_{j=1}^N (\boldsymbol{\mu}_j)_z \hat{\boldsymbol{z}} \\ \Rightarrow \boldsymbol{\tau}_k^{slabsum} &= -\frac{4\pi}{V} \sum_{j=1}^N (\boldsymbol{\mu}_k) \times (\boldsymbol{\mu}_j)_z \hat{\boldsymbol{z}} \end{aligned}$$

where $\hat{\boldsymbol{z}}$ is a unit vector in the z axis direction introduced to account for the fact that we are differentiating with respect to the z component of $\boldsymbol{\mu}_k$ only.

Finally, we look at the torque contribution from the ELC term added to allow us to work in this geometry:

$$\begin{aligned}
\mathbf{E}_k^{ELC} &= -\frac{\partial(U_k^{ELC})}{\partial\boldsymbol{\mu}_k} \\
&= -\frac{\partial(U_k^{ELC})}{\partial\boldsymbol{\mu}_k^\gamma}\widehat{\boldsymbol{\mu}}_k^\gamma - \frac{\partial(U_k^{ELC})}{\partial\mu_k^z}\widehat{\boldsymbol{\mu}}_k^z \\
&= \frac{2\pi}{L_x L_y} \sum_{\mathbf{G}_\gamma \neq 0} \frac{1}{G_\gamma (e^{G_\gamma L_z} - 1)} \sum_{j=1}^N \left\{ \frac{\partial}{\partial\boldsymbol{\mu}_k^\gamma} [S_{+,k}(\mathbf{G}_\gamma)S_{-,j}^*(\mathbf{G}_\gamma) + S_{-,k}(\mathbf{G}_\gamma)S_{+,j}^*(\mathbf{G}_\gamma)] \widehat{\boldsymbol{\mu}}_k^\gamma \right. \\
&\quad \left. + \frac{\partial}{\partial\mu_k^z} [S_{+,k}(\mathbf{G}_\gamma)S_{-,j}^*(\mathbf{G}_\gamma) + S_{-,k}(\mathbf{G}_\gamma)S_{+,j}^*(\mathbf{G}_\gamma)] \widehat{\boldsymbol{\mu}}_k^z \right\} \quad (65)
\end{aligned}$$

where $\widehat{\boldsymbol{\mu}}_k^z$ and $\widehat{\boldsymbol{\mu}}_k^\gamma$ are directed unit vectors. The derivative with respect to $\boldsymbol{\mu}_k^\gamma$ of $S_{\pm,k}(\mathbf{G}_\gamma)$ is:

$$\frac{\partial}{\partial\boldsymbol{\mu}_k^\gamma}(S_{k\pm}(\mathbf{G}_\gamma)) = e^{i\mathbf{G}_\gamma \cdot \boldsymbol{\gamma}_k} e^{\pm G_\gamma z_k} (i\mathbf{G}_\gamma).$$

From which we get:

$$\begin{aligned}
\frac{\partial}{\partial\boldsymbol{\mu}_k^\gamma} S &= S_{-,j}^*(\mathbf{G}_\gamma) \frac{\partial}{\partial\boldsymbol{\mu}_k^\gamma} S_{+,k}(\mathbf{G}_\gamma) + S_{+,j}^*(\mathbf{G}_\gamma) \frac{\partial}{\partial\boldsymbol{\mu}_k^\gamma} S_{-,k}(\mathbf{G}_\gamma) \\
&= (-i\boldsymbol{\mu}_j^\gamma \cdot \mathbf{G}_\gamma - \mu_j^z \cdot G_\gamma) e^{-i\mathbf{G}_\gamma \cdot \boldsymbol{\gamma}_j} e^{-G_\gamma z_j} e^{i\mathbf{G}_\gamma \cdot \boldsymbol{\gamma}_k} e^{G_\gamma z_k} (i\mathbf{G}_\gamma) \\
&\quad + (-i\boldsymbol{\mu}_j^\gamma \cdot \mathbf{G}_\gamma + \mu_j^z \cdot G_\gamma) e^{-i\mathbf{G}_\gamma \cdot \boldsymbol{\gamma}_j} e^{G_\gamma z_j} e^{i\mathbf{G}_\gamma \cdot \boldsymbol{\gamma}_k} e^{-G_\gamma z_k} (i\mathbf{G}_\gamma) \\
&= [(-i\boldsymbol{\mu}_j^\gamma \cdot \mathbf{G}_\gamma - \mu_j^z \cdot G_\gamma) e^{G_\gamma z_{kj}} + (-i\boldsymbol{\mu}_j^\gamma \cdot \mathbf{G}_\gamma + \mu_j^z \cdot G_\gamma) e^{G_\gamma z_{jk}}] (i\mathbf{G}_\gamma) e^{i\mathbf{G}_\gamma \cdot \boldsymbol{\gamma}_{kj}} \quad (66)
\end{aligned}$$

where S , $\boldsymbol{\gamma}_{kj}$ and z_{kj} are as defined for the force calculations in §5.3.1. Differentiating $S_{\pm,k}(\mathbf{G}_\gamma)$ with respect to μ_k^z gives:

$$\frac{\partial}{\partial\mu_k^z}(S_{k\pm}(\mathbf{G}_\gamma)) = e^{i\mathbf{G}_\gamma \cdot \boldsymbol{\gamma}_k} e^{\pm G_\gamma z_k} (\pm G_\gamma).$$

So we have

$$\begin{aligned}
\frac{\partial}{\partial\mu_k^z} S_k &= S_{-,j}^*(\mathbf{G}_\gamma) \frac{\partial}{\partial\mu_k^z} S_{+,k}(\mathbf{G}_\gamma) + S_{+,j}^*(\mathbf{G}_\gamma) \frac{\partial}{\partial\mu_k^z} S_{-,k}(\mathbf{G}_\gamma) \\
&= (-i\boldsymbol{\mu}_j^\gamma \cdot \mathbf{G}_\gamma - \mu_j^z \cdot G_\gamma) e^{-i\mathbf{G}_\gamma \cdot \boldsymbol{\gamma}_j} e^{-G_\gamma z_j} e^{i\mathbf{G}_\gamma \cdot \boldsymbol{\gamma}_k} e^{G_\gamma z_k} G_\gamma \\
&\quad + (-i\boldsymbol{\mu}_j^\gamma \cdot \mathbf{G}_\gamma + \mu_j^z \cdot G_\gamma) e^{-i\mathbf{G}_\gamma \cdot \boldsymbol{\gamma}_j} e^{G_\gamma z_j} e^{i\mathbf{G}_\gamma \cdot \boldsymbol{\gamma}_k} e^{-G_\gamma z_k} (-G_\gamma) \\
&= [(-i\boldsymbol{\mu}_j^\gamma \cdot \mathbf{G}_\gamma - \mu_j^z \cdot G_\gamma) G_\gamma e^{G_\gamma z_{kj}} + (-i\boldsymbol{\mu}_j^\gamma \cdot \mathbf{G}_\gamma + \mu_j^z \cdot G_\gamma) (-G_\gamma) e^{G_\gamma z_{jk}}] e^{i\mathbf{G}_\gamma \cdot \boldsymbol{\gamma}_{kj}}. \quad (67)
\end{aligned}$$

Substituting (66) and (67) into (65) then gives

$$\begin{aligned} \mathbf{E}_k^{ELC} = & \frac{2\pi}{L_x L_y} \sum_{\mathbf{G}_\gamma \neq 0} \frac{1}{G_\gamma (e^{G_\gamma L_z} - 1)} \sum_{j=1}^N \left\{ [(-i\boldsymbol{\mu}_j^\gamma \cdot \mathbf{G}_\gamma - \mu_j^z \cdot G_\gamma) e^{G_\gamma z_{kj}} + (-i\boldsymbol{\mu}_j^\gamma \cdot \mathbf{G}_\gamma + \mu_j^z \cdot G_\gamma) e^{G_\gamma z_{jk}}] \right. \\ & \times (i\mathbf{G}_\gamma) e^{i\mathbf{G}_\gamma \cdot \boldsymbol{\gamma}_{kj}} \widehat{\boldsymbol{\mu}}_k^\gamma + [(-i\boldsymbol{\mu}_j^\gamma \cdot \mathbf{G}_\gamma - \mu_j^z \cdot G_\gamma) G_\gamma e^{G_\gamma z_{kj}} + (-i\boldsymbol{\mu}_j^\gamma \cdot \mathbf{G}_\gamma + \mu_j^z \cdot G_\gamma) (-G_\gamma)] \\ & \left. \times e^{G_\gamma z_{jk}} e^{i\mathbf{G}_\gamma \cdot \boldsymbol{\gamma}_{kj}} \widehat{\boldsymbol{\mu}}_k^z \right\}. \end{aligned}$$

Hence, the contribution to the torque from the ELC term is found by taking the cross product of \mathbf{E}_k^{ELC} with $\boldsymbol{\mu}_k$ as follows

$$\begin{aligned} \boldsymbol{\tau}_k^{ELC} = & \frac{2\pi}{L_x L_y} \sum_{\mathbf{G}_\gamma \neq 0} \frac{1}{G_\gamma (e^{G_\gamma L_z} - 1)} \sum_{j=1}^N \left\{ \boldsymbol{\mu}_k \times [(-i\boldsymbol{\mu}_j^\gamma \cdot \mathbf{G}_\gamma - \mu_j^z \cdot G_\gamma) e^{G_\gamma z_{kj}} \right. \\ & + (-i\boldsymbol{\mu}_j^\gamma \cdot \mathbf{G}_\gamma + \mu_j^z \cdot G_\gamma) e^{G_\gamma z_{jk}}] (i\mathbf{G}_\gamma) e^{i\mathbf{G}_\gamma \cdot \boldsymbol{\gamma}_{kj}} \widehat{\boldsymbol{\mu}}_k^\gamma + \boldsymbol{\mu}_k \times [(-i\boldsymbol{\mu}_j^\gamma \cdot \mathbf{G}_\gamma - \mu_j^z \cdot G_\gamma) G_\gamma e^{G_\gamma z_{kj}} \\ & \left. + (-i\boldsymbol{\mu}_j^\gamma \cdot \mathbf{G}_\gamma + \mu_j^z \cdot G_\gamma) (-G_\gamma) e^{G_\gamma z_{jk}}] e^{i\mathbf{G}_\gamma \cdot \boldsymbol{\gamma}_{kj}} \widehat{\boldsymbol{\mu}}_k^z \right\}. \end{aligned}$$

The overall torque is then given by summing the various components discussed in this section:

$$\boldsymbol{\tau}_k^{slab} = \boldsymbol{\tau}_k^r + \boldsymbol{\tau}_k^{slabk} + \boldsymbol{\tau}_k^{slabsum} + \boldsymbol{\tau}_k^{ELC}.$$

As mentioned previously the results in this section are a discussion of possibilities only as I was unable to verify the results contained within in the absence of numerical work.

5.4 Errors in Ewald Method for a Confined Geometry

Clearly, the real space errors are as detailed in §3.3 as the real space term (and hence its force and torque have not changed). The reciprocal space errors can also be obtained by taking those derived in the standard geometry and replacing k with G and \mathbf{K} with \mathbf{G} . So, neither of these results is recounted here although Bródka^[5] observes that the real space error is likely to be overestimated since it takes into account all of the space in the simulation box even though some parts of it are empty of particles.

It is of more interest for us to look at the contribution to the error from the ELC term added to deal with a confined geometry. This term contributes to the error since it is heavily dependent on the reciprocal space variables G and \mathbf{G} , which means that the choice of k_c , where k_c is the reciprocal space cut-off as before, will affect this term. In fact the cut-off in relation to this term is taken to be $G_c = \frac{2\pi k_c}{L_x}$ [5]. Bródka^[5] provides details of the error calculations for U^{ELC} and the results in this section are taken from his work.

As we found for the reciprocal space term in three dimensional geometry there are different contributions to the error from the diagonal and off diagonal terms and the overall error contribution is taken to be the sum of these. Using (61) and making substitutions

(as in §3.3) by employing a spherical co-ordinate system allows Bródka^[5] to state the following:

$$\begin{aligned}\Delta U_{i,off}^{ELC} &= -\frac{4\pi}{L_x L_y} \sum_{\substack{\mathbf{G} \\ G > G_c}} \frac{G}{e^{GL_z} - 1} \{ \sin^2 \theta \cos \omega(\boldsymbol{\mu}_i^\gamma, \mathbf{G}) \cos \omega(\boldsymbol{\mu}_j^\gamma, \mathbf{G}) \cos(\mathbf{G} \cdot \boldsymbol{\gamma}_{ij}) \cosh(Gz_{ij}) \\ &\quad + [\sin \theta \cos \theta \cos \omega(\boldsymbol{\mu}_i^\gamma, \mathbf{G}) + \sin \theta \cos \theta \cos \omega(\boldsymbol{\mu}_j^\gamma, \mathbf{G})] \sin(\mathbf{G} \cdot \boldsymbol{\gamma}_{ij}) \sinh(G\gamma_{ij}) \\ &\quad - \cos^2 \theta \cos(\mathbf{G} \cdot \boldsymbol{\gamma}_{ij}) \cosh(Gz_{ij}), \\ \Delta U_{i,diag}^{ELC} &= -\frac{2\pi}{L_x L_y} \sum_{\substack{\mathbf{G} \\ G > G_c}} \frac{G}{e^{GL_z} - 1} [\sin^2 \theta \cos^2 \omega(\boldsymbol{\mu}_i^\gamma, \mathbf{G}) - \cos^2 \theta].\end{aligned}$$

Following this it is again assumed that the positions and orientations are uncorrelated and so the relationships given in (44) can be used to simplify the results above. Making use of the Kronecker delta function and then taking the averages under the assumption of no correlation gives^[5]

$$\begin{aligned}\langle (\Delta U_{i,off}^{ELC})^2 \rangle &= -\left(\frac{\pi \mu^2}{L_x L_y} \right)^2 \sum_{\substack{\mathbf{G} \\ G > G_c}} \frac{G^2}{(e^{GL_z} - 1)^2} \{ [\cos^2 \omega(\boldsymbol{\mu}_i^\gamma, \mathbf{G}) \cos^2 \omega(\boldsymbol{\mu}_j^\gamma, \mathbf{G}) + 1] \langle \cosh^2(Gz_{ij}) \rangle \\ &\quad + [\cos^2 \omega(\boldsymbol{\mu}_i^\gamma, \mathbf{G}) + \cos^2 \omega(\boldsymbol{\mu}_j^\gamma, \mathbf{G})] \langle \sinh^2(G\gamma_{ij}) \rangle \},\end{aligned}\quad (68)$$

$$\langle \Delta U_{i,diag}^{ELC} \rangle = -\frac{\pi}{L_x L_y} \mu^2 \sum_{\substack{\mathbf{G} \\ G > G_c}} \frac{G}{e^{GL_z} - 1} [\cos^2 \omega(\boldsymbol{\mu}_i^\gamma, \mathbf{G}) - 1].\quad (69)$$

In the continuation of this calculation Bródka^[5] rewrites (68) and (69) in integral notation and then evaluates these analytically. Finally he combines the diagonal and off diagonal terms using the following formula for the error of the ELC term in the total potential energy:

$$\Delta U^{ELC} \approx \sqrt{\frac{1}{2} \sum_{i=1}^N \sum_{\substack{j=1 \\ j \neq i}}^N \langle (\Delta U_{i,off}^{ELC})^2 \rangle + \sum_{i=1}^N \langle \Delta U_{i,diag}^{ELC} \rangle}.$$

This results in an upper bound for the error of the ELC term given by

$$\begin{aligned}\Delta U^{ELC} &\approx \frac{N\mu^2}{4} \frac{1}{e^{GL_z} - 1} \left\{ g_2(G_c, L_z) + \frac{1}{2} \sqrt{\frac{\pi}{2L_x L_y}} \right. \\ &\quad \left. \times \sqrt{9e^{2G_c h} g_1(G_c, L_z - h) + 22g_1(G_c, L_z) + 9e^{2G_c h} g_1(G_c, L_z + h)} \right\}\end{aligned}$$

where

$$\begin{aligned}g_1(G, x) &= \frac{G^3}{x} + \frac{3G^2}{2x^2} + \frac{3G}{2x^3} + \frac{3}{4x^4}, \\ g_2(G, x) &= \frac{G^2}{x} + \frac{2G}{x^2} + \frac{2}{x^3},\end{aligned}$$

and h is taken to be the distance between two strips. Care has to be taken not to confuse h with H , which is the height of the strips (i.e. $H = L_z - h$).

The method employed by Bródka^[5] echoes the method used by Wang and Holm^[33] that was recounted in §3.3. As was demonstrated in the case of the Ewald method for a standard geometry the same process can be used to perform error calculations relating to the expressions for the force and torque. Once the ideas discussed in §5.3 have been developed error calculations and numerical work will test the accuracy of the results obtained. However, due to time restraints this has not been accomplished in this report.

6 Conclusion

This project has provided a comprehensive look at the theory surrounding the Ewald summation and its ability to model dipolar interactions. In any computer simulation the ability to decrease the running times and costs of programs is pivotal and this idea has been discussed throughout this report. The Ewald method itself is computationally effective but this effect can be enhanced by the use of fast Fourier transforms and optimising the parameters. Although this report does not generate new results other than discussions regarding the force and torque contribution from the electrostatic layer correction (ELC) term (as far as I could see such work has yet to be published) it provides a thorough background to the work that has been done previously. The knowledge gained from this provides a spring board to developing the ideas discussed and there is clearly an interest among scientists in furthering this field.

6.1 Further Work

Unfortunately due to the time constraints of this project I was unable to program the formulae discussed in relation to a slab geometry in order to simulate the behaviour here. However, I will continue to work in this area as part of my PhD studies with the aim of publishing any advances made. It will be of great value to use the methods discussed in §3.3 and §5.4 to perform and verify error calculations for the force and torque contributions from the ELC term in a confined geometry. As part of this I aim to discuss the optimisation of the parameters for dipolar interactions in a confined geometry.

Another obvious action will be to program the results given in §5 and once successful to look at the situations this model can be applied to. Its application in the modelling of shear stress in a system of latticed boxes is of particular interest. The Ewald summation cannot be used to model shearing in a system such as that described in §2.2 as creating shear between layers of simulation boxes destroys the periodicity inherent in the Ewald method. However, once we can apply the Ewald method to a confined geometry we can use this to our advantage. The walls created to simulate the slab geometry can be used to create the shear, leaving the structure of simulation boxes, and hence the periodicity of the system, unchanged. In initial simulations the top wall can be 'pulled along' at a steady rate to simulate steady shear and later simulations may model more sudden shear by 'pulling' the wall with more force. A further extension to this would be to use a sin function to simulate oscillation of the top wall and model the effect of this on the system. This will have similarities to the work of Wang et al.^[34] who modelled shear in electro-rheological (ER) fluids but were unable to implement the Ewald method owing to the restrictions described previously.

Appendix A List of Symbols

Most of the symbols included in this list are given in their general form only although many are used in conjunction with various subscripts and superscripts. The following notes give an idea of the subscripts and superscripts used, although it is not intended to be exhaustive.

Throughout this report a subscript c generally means that charge-charge interactions are being discussed whilst a subscript d refers to dipole-dipole interactions. If neither subscript is given it is likely to be dealing with dipolar interaction since no subscript is used in chapters dealing with these only. However, be wary as a subscript c is also used when discussing cut-offs for dipolar systems. Check the notes at the start of each section for further clarification. Other subscripts, such as i , j and k refer to individual particles whilst subscripts x , y or z refer to a symbol relating to an element of the co-ordinate system.

Superscripts are used to denote individual terms of an element that is usually obtained by summing all such terms. Superscript r refers to an expression in real space, whilst a symbol with superscript k is given in reciprocal space. Other superscripts used include *surf* to indicate surface terms and *self* to indicate terms of self-interaction. When referring to the confined geometry system the superscript of various components is modified to have the word *slab* in front.

A.1 Latin Alphabet

d dimensionality of the system

E electrostatic field

F force

H width of strips containing particles in confined geometry representation

k absolute value of \mathbf{k}

k_c cut-off in reciprocal space

\mathbf{k} Fourier space position in respect to the centre of the distribution

L length of the simulation box

M total dipole moment

\mathbf{n} vector representing the simulation box

n_s number of clusters of size s

N number of particles in the simulation box

q a charge

r absolute value of \mathbf{r}

r_c cut-off in real space

\mathbf{r} position

\mathbf{r}_{ij} distance between particles i and j given to be $\mathbf{r}_i - \mathbf{r}_j$

T total computing time

U potential energy of particle-particle interactions

V volume of simulation box

A.2 Greek Alphabet

α Ewald splitting parameter that describes the width of the Gaussian charge distribution

γ_{ij} projection of \mathbf{r}_{ij} into (x, y) plane

δ required accuracy

ΔF error in the force calculation

$\Delta\tau$ error in the torque calculation

$\Delta\tau$ error in the potential energy calculation

$\Delta\Theta$ cut-off error for dipolar Ewald summation

ϵ_0 permittivity of free space

ϵ_s relative permittivity (dielectric constant)

λ dipolar coupling constant

$\boldsymbol{\mu}$ a dipole

ρ^{charge} Gaussian charge distribution used in derivation of Ewald summation

$\hat{\rho}^{charge}$ Fourier transform of ρ^{charge}

σ particle size

$\boldsymbol{\tau}$ torque

ϕ volume fraction of particles

χ direction and magnitude of a pair-potential's contribution to error

ω the angle between two vectors

Appendix B Glossary

Brownian motion The presumably random drifting of particles that are suspended in a fluid.

charge A unit of matter which is either positive (contains more protons than electrons) or negative (contains more electrons than protons).

colloid A substance dispersed microscopically throughout another substance. In this project we look at magnetic particles dispersed in liquid.

colloidal suspension A material that possesses attributions of more than one state of matter.

complementary error function (denoted by $erfc(x)$) The complement of the Gaussian error function given by $1 - erf(x)$.

Coulomb's law A law describing the electrostatic interaction between charged particles. In scalar form it is $\frac{z_i z_j}{4\pi\epsilon_0 r^2}$.

coupling constant A measurement of the strength of the force involved in an interaction.

dipole A unit of matter that is negatively charged at one pole and positively charged at the opposite pole.

electro-rheological (ER) fluid A fluid that changes behaviour when an electrical field is applied.

electrostatic interaction An interaction between charged particles.

ferrofluid A fluid with nanometric particles that changes behaviour when a magnetic field is applied.

free space A perfect vacuum used in theoretical physics to discuss idealised situations.

Gauss error function (denoted by $erf(x)$) A special function used in measurement theory; its use in other areas of maths is not related to errors in measurements except by name.

long range interaction A spatial interaction that decays at a rate no faster than r^{-d} , where r is the molecular separation and d is the dimensionality of the system^[1].

magneto-rheological (MR) fluid A fluid with micrometric particles that changes behaviour when a magnetic field is applied.

microcanonical ensemble (NVE) A system where the moles (N), volume (V) and energy (E) remain constant over time.

minimum image convention A form of periodic boundary conditions whereby each particle only reacts with the closest image of each of the remaining particles.

molecular dynamics A computer simulation method used to solve Newton's laws of motion.

Newtonian fluid A fluid that can be categorised by its viscosity at a certain temperature.

pair potential The potential energy between two interacting objects.

permittivity The measure of resistance when an electric field is formed in a given medium.

point charge An idealised zero dimensional particle used to represent an object when the size and shape is irrelevant in the given context.

potential energy The energy of an object or system affected by position.

reciprocal space (also called k-space) The space in which Fourier transforms are represented.

rheology An area of physics involving the study of the deformation and flow of non-Newtonian fluids.

screened charge A point charge that has been damped by a surrounding field of charges.

shear stress A stress that arises as a result of force applied parallel to the cross section studied.

torque The tendency of a force to rotate an object about an axis.

References

- [1] M. P. Allen and D. J. Tildesley. *Computer Simulations of Liquids*. Oxford University Press, Oxford, 1987.
- [2] Axel Arnold, Jason de Joannis, and Christian Holm. Electrostatics in periodic slab geometries. I. *Journal of Chemical Physics*, 117(6):2496–2502, August 2002.
- [3] Ronald N. Bracewell. *The Fourier Transform and Its Applications*. McGraw-Hill Incorporated, London, second edition, 1978.
- [4] A. Bródka. Comment on “Electrostatics in periodic slab geometries. I”. *Journal of Chemical Physics*, 121(14):7032–7034, October 2004.
- [5] A. Bródka. Ewald summation method with electrostatic layer correction for interactions of point dipoles in slab geometry. *Chemical Physics Letters*, 400(1-3):62–67, December 2004.
- [6] A. Bródka. Optimal parameter values of the Ewald method with electrostatic layer correction for Coulomb interactions in slab geometry. *Journal of Molecular Structure*, 792-793:56–61, April 2006.
- [7] A. Bródka and A. Grzybowski. Electrostatic interactions in computer simulations of a three-dimensional system periodic in two directions: Ewald-type summation. *Molecular Physics*, 117(18):8208–8211, November 2002.
- [8] Juan J. Cerdà, Ekaterina Elfimova, V. Ballenegger, Ekaterina Krutikova, Alexey Ivanov, and Christian Holm. Study of the structure factor anisotropy and long range correlations of ferrofluids in the dilute low-coupling regime. *Journal of Magnetism and Magnetic Materials*, 323(10):1246–1253, .
- [9] Juan J. Cerdà, Sofia Kantorovich, and Christian Holm. Aggregate formation in ferrofluid monolayers: Simulations and theory. *Journal of Physics: Condensed Matter*, 20(20):1204125, .
- [10] Min-Feng Chung and Chao-Ming Fu. Optical transmittance and dynamic properties of ferrofluids (Fe_3O_4) under dc-biased magnetic fields. *IEEE Transactions on Magnetics*, 47(10):3170–3172, October 2011.
- [11] S. W. De Leeuw, J. W. Perram, and E. R. Smith. Simulation of electrostatic systems in periodic boundary conditions. I. Lattice sums and dielectric constants. *Proceedings of the Royal Society London A*, 373:57–66, October 1980.
- [12] Daan Frenkel and Berend Smit. *Understanding Molecular Simulations: From Algorithms to Application*. Academic Press Limited, London, 1996.

- [13] Matteo Frigo and Steven G. Johnson. FFTW, Accessed: August 2012. URL <http://www.fftw.org/>.
- [14] Andrew Gibbs. Molecular dynamics simulation of self-healing polymers. Master's thesis, University of Reading, Reading, March 2011.
- [15] A. Grzybowski and A. Bródka. Computationally efficient method for summing interactions of point dipoles in three dimensions with two-dimensional periodicity. *Chemical Physics Letters*, 361(3-4):329–333, July 2002.
- [16] Hadi Hezaveh, Alireza Fazlali, and Iman Noshadi. Synthesis, rheological properties and magnetoviscos effect of Fe_2O_3 / paraffin ferrofluids. *Journal of the Taiwan Institute of Chemical Engineers*, 43(1):159–164, January 2012.
- [17] Alan Hinchliffe. *Molecular Modelling for Beginners*. John Wiley & Sons Ltd, Chichester, 2003.
- [18] William Humphrey, Andrew Dalke, and Klaus Schulten. Vmd: Visual molecular dynamics. *Journal of Molecular Graphics*, 400(1-3):62–67, December 2004.
- [19] Alexey O. Ivanov, Zuowei Wang, and Christian Holm. Applying the chain formation model to magnetic properties of aggregated ferrofluids. *Physical Review E*, 69(3):031206.
- [20] Alexey O. Ivanov, Sofia S. Kantorovich, Evgeniy N. Reznikov, Christian Holm, Alexander F. Pshenichnikov, Alexander V. Lebedev, Alexandros Chremos, and Philip J. Camp. Magnetic properties of polydisperse ferrofluids: A critical comparison between experiment, theory, and computer simulation. *Physical Review E*, 75(6):061405, June 2007.
- [21] Sofia Kantorovich, Juan J. Cerdà, and Christian Holm. Microstructure analysis of monodisperse ferrofluid monolayers: Theory and simulation. *Physical Chemistry Chemical Physics*, 10(14):1883–1895, .
- [22] Sofia Kantorovich, Rudolf Weeber, Juan J. Cerdà, and Christian Holm. Ferrofluids with shifted dipoles: Ground state structures. *Soft Matter*, 7(11):5217–5227, .
- [23] Andrew R. Leach. *Molecular Modelling: Principles and Applications*. Pearson Education Limited, Dorchester, second edition, 2001.
- [24] J. López, L. F. González-Bahamón, J. Prado, J. C. Caicedo, G. Zambrano, M. E. Gómez, J. Esteve, and P. Prieto. Study of magnetic and structural properties of ferrofluids based on cobalt-zinc ferrite nanoparticles. *Journal of Magnetism and Magnetic Materials*, 324(5):394–402, March 2012.

- [25] Modesto T. López-López, Ana Gómez-Ramírez, Laura Rodríguez-Arco, Juan D. G. Durán, Larisa Iskakova, and Andrey Zubarev. Colloids on the frontier of ferrofluids. Rheological properties. *Langmuir*, 28(15):6232–6245, March 2012.
- [26] M. Mohebi, N. Jamasbi, and Jing Liu. Simulation of the formation of nonequilibrium structures in magnetorheological fluids subject to an external magnetic field. *Physical Review E*, 54(5):5407–5413.
- [27] K. W. Morton and D. F. Mayers. *Numerical Solution of Partial Differential Equations*. Cambridge University Press, Cambridge, 1994.
- [28] Nneoma Ogbonna. Molecular dynamics simulation. Master’s thesis, African Institute for Mathematical Sciences, Muizenberg, South Africa, May 2004.
- [29] William H. Press, Saul A. Teukolsky, William T. Vetterling, and Brian P. Flannery. *Numerical Recipes in C++*. Cambridge University Press, Cambridge, second edition, 2002.
- [30] Elena Pyanzina, Sofia Kantorovich, Juan J. Cerdà, and Christian Holm. Structure factor of ferrofluids with chain aggregates: Theory and computer simulations. *Journal of Magnetism and Magnetic Materials*, 323(10):1263–1268.
- [31] Jason P. Rich, Gareth H. McKinley, and Patrick S. Doyle. Arrested chain growth during magnetic directed particle assembly in yield stress matrix fluids. *Langmuir*, 28(8):3683–3689, February 2012.
- [32] E. R. Smith and J. W. Perram. Thermodynamic limit for a system with dipole-dipole interactions. *The Journal of the Australian Mathematical Society (Series B)*, 19(1):116–128, June 1975.
- [33] Zuowei Wang and Christian Holm. Estimate of the cutoff errors in the Ewald summation for dipolar systems. *Journal of Chemical Physics*, 115(14):6351, October 2001.
- [34] Zuowei Wang, Zhifang Lin, and Ruibao Tao. Structure and viscoelasticity of an electrorheological fluid in oscillatory shear: Computer simulation investigation. *Journal of Physics D: Applied Physics*, 30(8):1265–1271, April 1997.
- [35] Zuowei Wang, Christian Holm, and Hanns Walter Müller. Molecular dynamics study on the equilibrium magnetization properties and structure of ferrofluids. *Physical Review E*, 66(2):021405, August 2002.
- [36] In-Chul Yeh and Max L. Berkowitz. Ewald summation for systems with slab geometry. *Journal of Chemical Physics*, 111(7):3155–3162.